Chapter 4

M-ary Optical Computing

Jian Wang and Yun Long

Additional information is available at the end of the chapter

http://dx.doi.org/10.5772/67351

Abstract

The era of cloud computing has fuelled the increasing demand on data centers for high-performance, high-speed data storage and computing. Digital signal processing may find applications in future cloud computing networks containing a large sum of data centers. Addition and subtraction are considered to be fundamental building blocks of digital signal processing which are ubiquitous in microprocessors for arithmetic operations. However, the processing speed is limited by the electronic bottleneck. It might be valuable to implement high-speed arithmetic operations of addition and subtraction in the optical domain. In this chapter, recent results of M-ary optical arithmetic operations for high base numbers are presented. By exploiting degenerate and nondegenerate four-wave mixing (FWM) in highly nonlinear fibers (HNLFs), graphene-assisted optical devices, and silicon waveguide devices, various types of two-/three-input high-speed quaternary/octal/decimal/hexadecimal optical computing operations have been demonstrated. Operation speed up to 50 Gbaud of this computing approach is experimentally examined. The demonstrated M-ary optical computing using high base numbers may facilitate advanced data management and superior network performance.

Keywords: high-base optical signal processing, multilevel modulation format, four-wave mixing, wavelength conversion, optical computing

1. Introduction

The great progress of fiber-optic communication has driven the success in transmitting/receiving very high-speed data signals in optical fiber links [1–5]. Recently, the era of cloud computing has fuelled the increasing demand on data centers for high-performance, high-speed data storage and computing. Optical interconnection is considered to be a promising technology for data interconnection in data centers. In future cloud computing networks containing a large sum of data centers, optical technology will play an important part [6–8]. For inter-data

center communication, modern optical communication links will be used. Advanced modulation formats and wavelength division multiplex (WDM) can be used to enhance the transmission capacity of inter-data center links. And for intra-data center links, low-cost short-reach optical interconnection technologies, such as vertical-cavity surface-emitting laser (VCSEL) and multimode fiber, will be adopted. The rapid development of optical interconnection in data centers has also promoted increasing interest for digital signal processing used in data centers for wavelength management or routing. Among various digital signal processing operations, two important arithmetic modules, i.e., addition and subtraction, are considered to be fundamental building blocks of digital signal processing which are ubiquitous in microprocessors for arithmetic operations. However, the processing speed is limited by the electronic bottleneck. It might be valuable to implement high-speed arithmetic operations of addition and subtraction in the optical domain.

Remarkably, nonlinear optics has offered great potential to develop high-speed optical signal processing using optical nonlinearities [9–21]. Multitudinous optical signal processing functionalities have been demonstrated. Commonly used optical signal processing functionalities include wavelength (de)multiplexing, wavelength conversion, data exchange, optical addressing, optical switching, optical logic gate and computing, optical format conversion, optical equalization, tunable optical delay, optical regeneration, optical coding/decoding, and more [22–54]. As depicted in **Figure 1**, the material platforms for nonlinear optical signal processing mainly include highly nonlinear fiber (HNLF) [51, 55–57], semiconductor optical amplifier (SOA) [58–60], periodically poled lithium niobate (PPLN) waveguide [32, 35, 36, 61, 62], chalcogenide (As_2S_3) waveguide [63], silicon waveguide [64–66], and graphene-assisted device [67]. Previously, optical arithmetic or optical logic operations have been reported in these material systems. It is noted that most of previous research efforts are dedicated to optical computing for binary modulation formats such as on-off keying (OOK) and binary phase-shift keying (BPSK). Despite favorable operation performance achieved for binary operation, it suffers the limited bit rate and low spectral efficiency because each symbol for binary modulation formats only carries single-bit information.

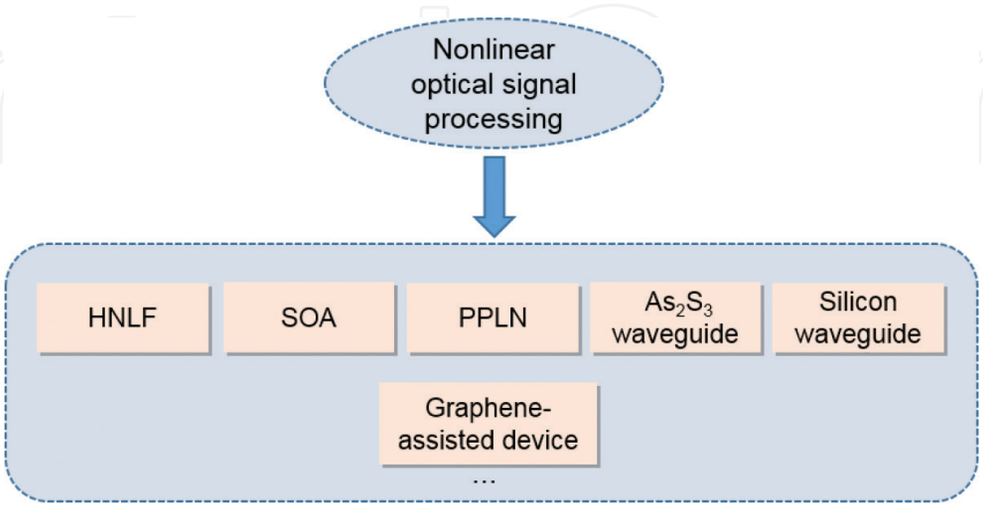

Figure 1. Material classification for nonlinear optical signal processing.

The use of M-ary phase-shift keying (m-PSK) and M-ary quadrature amplitude modulation (m-QAM) in coherent systems has become a key technique for efficient increase of the transmission capacity and spectral efficiency of optical communication systems. For instance, quadrature phase-shift keying (QPSK) with 2-bit information in one symbol has been extensively used in high-speed optical fiber transmission systems [68, 69]. Multilevel modulation format containing multiple constellation points in the constellation diagram can also be used to represent M-ary numbers. Taking QPSK as an example, four constellation points (i.e., four-phase levels) in the constellation diagram of QPSK signal can donate a quaternary base number (i.e., 0, 1, 2, 3), as shown in **Figure 2**. Similarly, 8 PSK (16 PSK) signal which has 8 (16) points in its constellation plane can represent an octal (hexadecimal) base number. The related optical signal processing functions to multilevel modulation formats could be addition and subtraction of high base numbers. In this scenario, a laudable goal would be to perform addition and subtraction of high base numbers because (i) high capacities might be achievable, (ii) optical spectra might be utilized efficiently, and (iii) processing throughput might be improved.

In this chapter, we tend to provide a comprehensive report of our recent research works on M-ary optical computing for multilevel modulation formats by exploiting optical nonlinearities [70–75]. Various material platforms, including HNLFs, graphene-assisted optical devices, and silicon waveguide devices, are adopted to performing high-speed M-ary addition and subtraction. First, we report the experimental results of optical addition and subtraction using HNLFs. Functionalities of quaternary addition/subtraction are examined. Second, we show the graphene-enhanced optical nonlinearities in graphene-assisted optical devices and its application in optical computing. Finally, we present the latest results of high-speed optical computing using ultra-compact on-chip silicon waveguides. Quaternary/hexadecimal hybrid optical computing is suc-

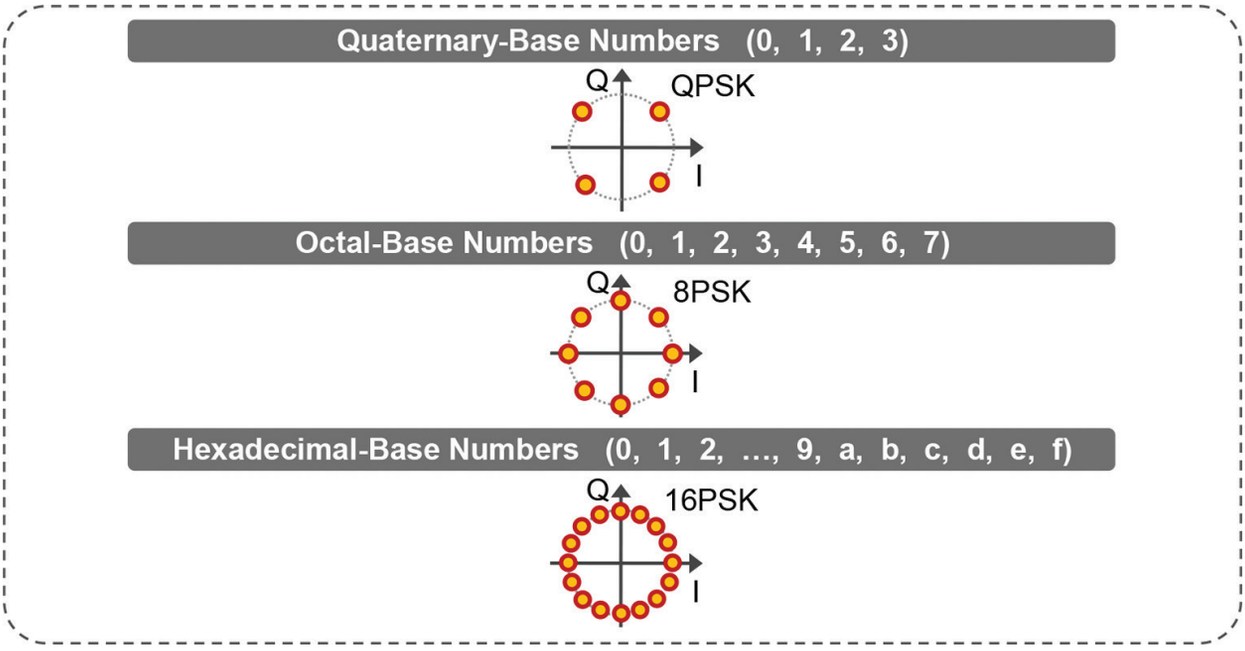

Figure 2. Schematic constellations of advanced multilevel modulation formats representing M-ary (quaternary, octal, hexadecimal) numbers (QPSK, 8PSK, 16PSK).

cessfully demonstrated in a complementary metal oxide semiconductor (CMOS)-compatible platform, which can be potentially integrated with standard CMOS large-scale integrated circuit.

2. Binary optical logic

In the last two decades, binary optical computing has been widely studied. Up to now, many schemes have been demonstrated to realize various elementary optical logic operations, including AND, OR, NOT, XOR, XNOR, NAND, and NOR [32, 55, 61, 62, 76–85]. By combining multiple elementary optical logic operations, advanced logic operations such as half-adder, half-subtractor, full-adder, and full-subtractor have also been proposed and demonstrated [36, 86–91]. **Figure 3** shows an example of simultaneous half-adder, half-subtractor, and OR logic gate [36].

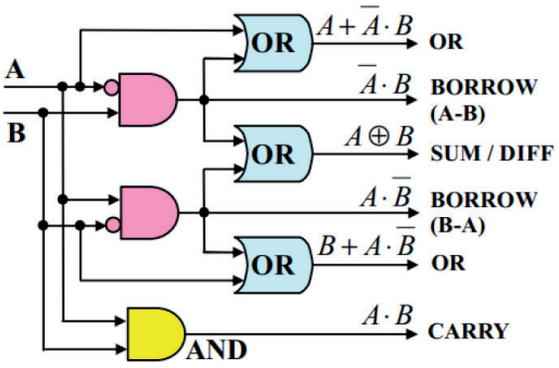

Input data bits		Adder (A+B)		Subtracter A-B/B-A			Logic gate
A	B	CAR.	SUM	BOR. A-B	BOR. B-A	DIFF.	OR
0	0	0	0	0	0	0	0
0	1	0	1	1	0	1	1
1	0	0	1	0	1	1	1
1	1	1	0	0	0	0	1

Figure 3. Digital gate-level diagram and logical truth table for simultaneous half-adder, half-subtractor, and OR logic gate.

Despite favorable operation performance of the binary operation, it still suffers from the limited bit rate and low spectral efficiency. Owing to the great success of advanced modulation format and coherent detection in optical communication, the implementation of M-ary optical computing becomes possible. Since the multiple constellation points in the complex plane of multilevel modulation format can be used to represent M-ary numbers, it is easy to extend binary optical computing to M-ary.

3. M-ary optical computing using HNLF

We propose and demonstrate M-ary optical computing of advanced multilevel modulation signals based on degenerate/nondegenerate FWM in HNLFs.

We first demonstrate high-speed two-input high-base optical computing (addition/subtraction/complement/doubling) of quaternary numbers using optical nonlinearities and (differential) quadrature phase-shift keying ((D)QPSK) signals. **Figure 4** illustrates the concept and

http://dx.doi.org/10.5772/67351

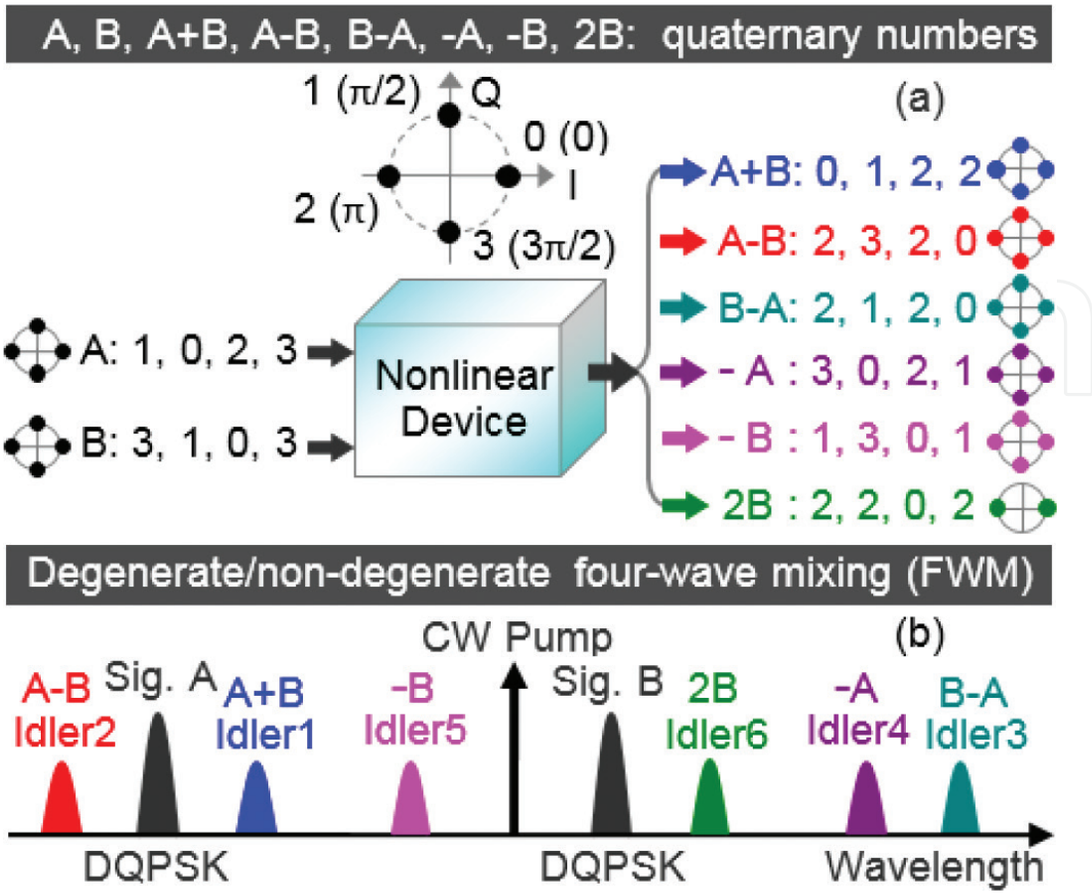

Figure 4. (a) Concept and (b) principle of two-input high-base optical computing (quaternary addition/subtraction/complement/doubling) using a single nonlinear device and (D)QPSK signals.

operation principle of the proposed quaternary addition/subtraction/complement/doubling. Four-phase levels of (D)QPSK signal represent quaternary numbers. Three nondegenerate FWMs and three degenerate FWMs in an HNLF are exploited to simultaneously implement multiple arithmetic functions. The input of the HNLF contains two (D)QPSK signals (*A, B*) and one continuous wave (CW) pump. Six converted idlers (idlers 1–6) are generated by three nondegenerate FWMs (idlers 1–3) and three degenerate FWMs (idlers 4–6). The relationships between the electrical field (E) and optical phase (Φ) under non-depletion approximation are expressed as

$$E_{i1} \propto E_A \cdot E_B \cdot E_{CW}^*, \quad \Phi_{i1} = \Phi_A + \Phi_B - \Phi_{CW} \tag{1}$$

$$E_{i2} \propto E_A \cdot E_B^* \cdot E_{CW}, \quad \Phi_{i2} = \Phi_A - \Phi_B + \Phi_{CW} \tag{2}$$

$$E_{i3} \propto E_A^* \cdot E_B \cdot E_{CW}, \quad \Phi_{i3} = \Phi_B - \Phi_A + \Phi_{CW} \tag{3}$$

$$E_{i4} \propto E_{CW} \cdot E_{CW} \cdot E_A^*, \quad \Phi_{i3} = 2\Phi_{CW} - \Phi_A \tag{4}$$

$$E_{i5} \propto E_{CW} \cdot E_{CW} \cdot E_B^*, \quad \Phi_{i5} = 2\Phi_{CW} - \Phi_B \tag{5}$$

$$E_{i6} \propto E_B \cdot E_B \cdot E_{CW}^*, \quad \Phi_{i6} = 2\Phi_B - \Phi_{CW} \tag{6}$$

Owing to the phase wrap characteristic with a periodicity of 2π, it is implied from Eqs. (1) to (6) that idlers 1–6 carry out modulo four operations of quaternary addition (A + B), dual-directional subtraction (A − B, B − A), complement (−A, −B), and doubling (2B), respectively.

Shown in **Figure 5** are measured spectra. Two 100-Gbit/s 2^7-1 RZ-(D)QPSK signals (A, 1546.6 nm; B, 1555.5 nm), and a CW pump (1553.2 nm), are launched into a 460-m HNLF. The low and flat dispersion of HNLF enables multiple FWM processes, and thus six idlers are obtained. The six idlers correspond to addition (A + B), subtraction (A − B, B − A), complement (−A, −B), and doubling (2B) of quaternary numbers (A, B), respectively.

We measured waveforms and balanced eyes of the demodulated in-phase (I) and quadrature (Q) components of two input 100-Gbit/s (D)QPSK signals and six converted idlers. The 100-Gbit/s (D)QPSK signal is demodulated using a delay-line interferometer (DLI) with a 20 ps delay difference between two arms. The obtained results are shown in **Figures 6** and **7**, which confirm the successful implementation of 50-Gbaud quaternary addition (A+B), dual-directional subtraction (A−B, B−A), complement (−A, −B), and doubling (2B) based on FWM in an HNLF.

Figure 8 shows the bit error rate (BER) curves. The power penalty is about 4 dB for addition, while 3 dB for subtraction, 2 dB for complement, and 3.1 dB for doubling at a BER of 10^{-9}. The measured constellations using an optical complex spectrum analyzer are shown in **Figure 9**. One can clearly see that addition (A+B) and subtraction (A−B, B−A) have four-phase levels (0, π/2, π, 3π/2), while doubling (2B) has only two-phase levels (0, π).

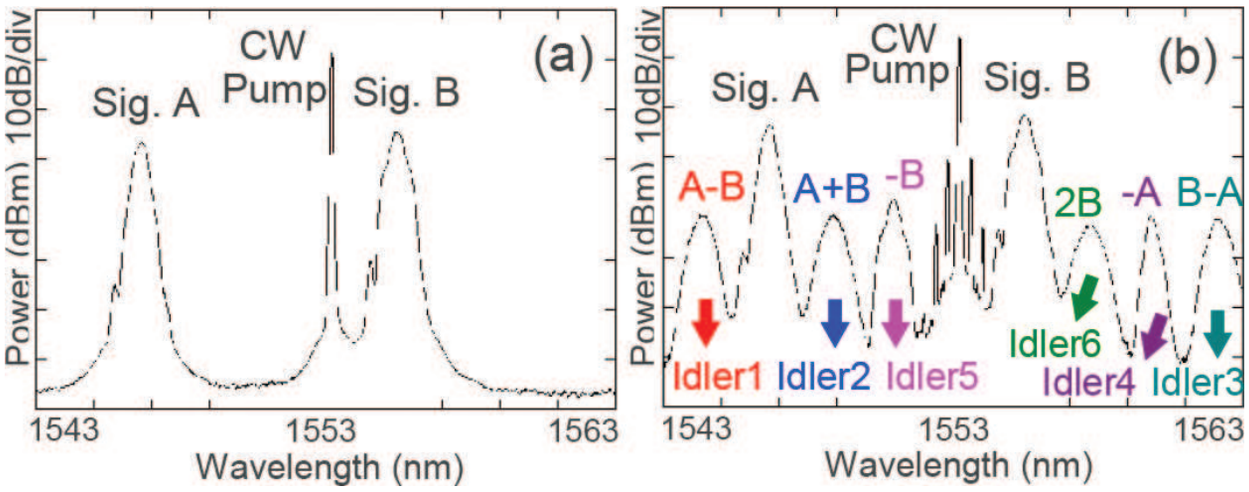

Figure 5. Measured spectra for 50-Gbaud two-input quaternary addition/subtraction/complement/doubling (a) before and (b) after HNLF.

http://dx.doi.org/10.5772/67351

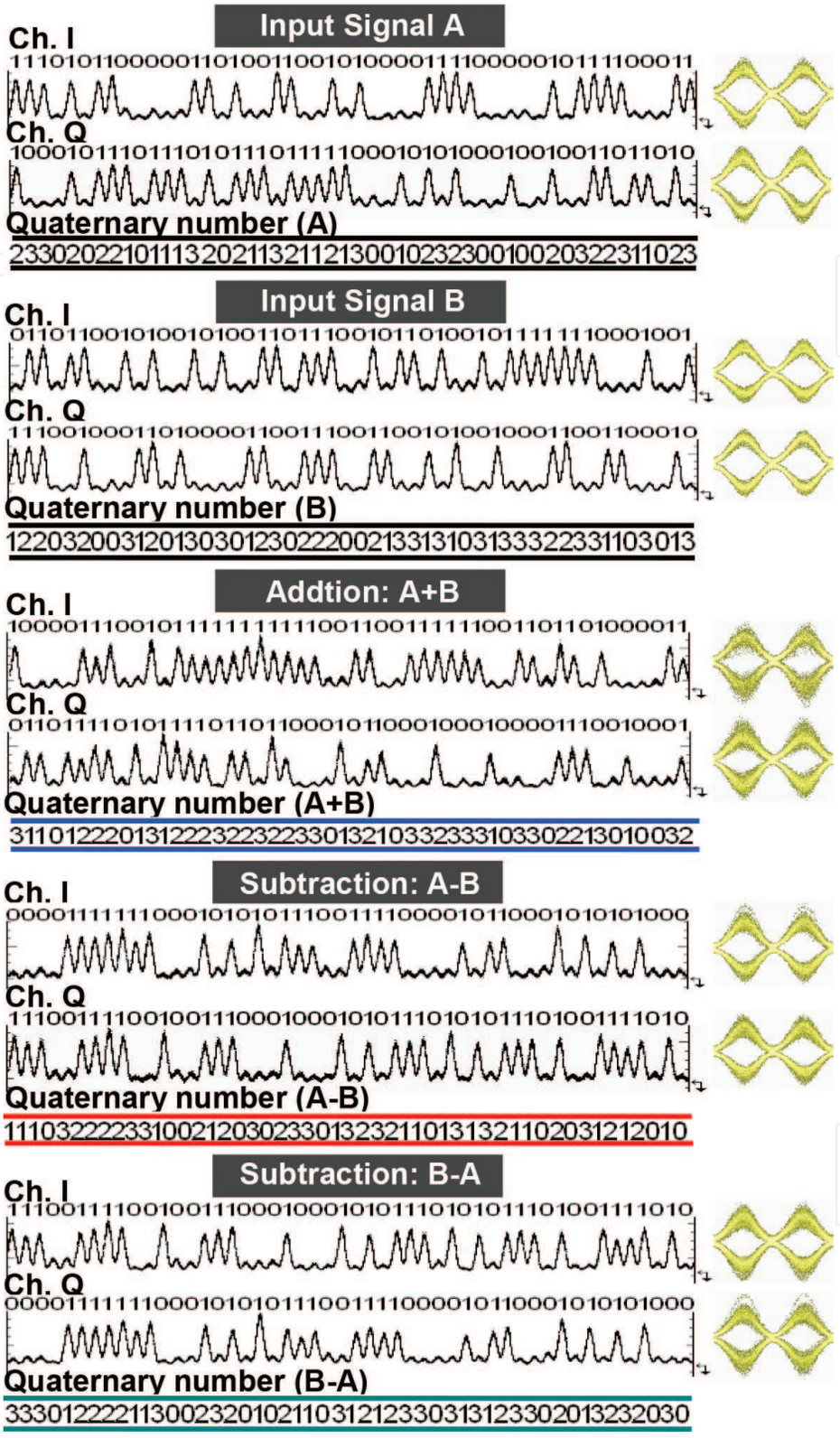

Figure 6. Demodulated waveforms and balanced eyes for 50-Gbaud two-input quaternary addition and dual-directional subtraction using 100-Gbit/s (D)QPSK signals.

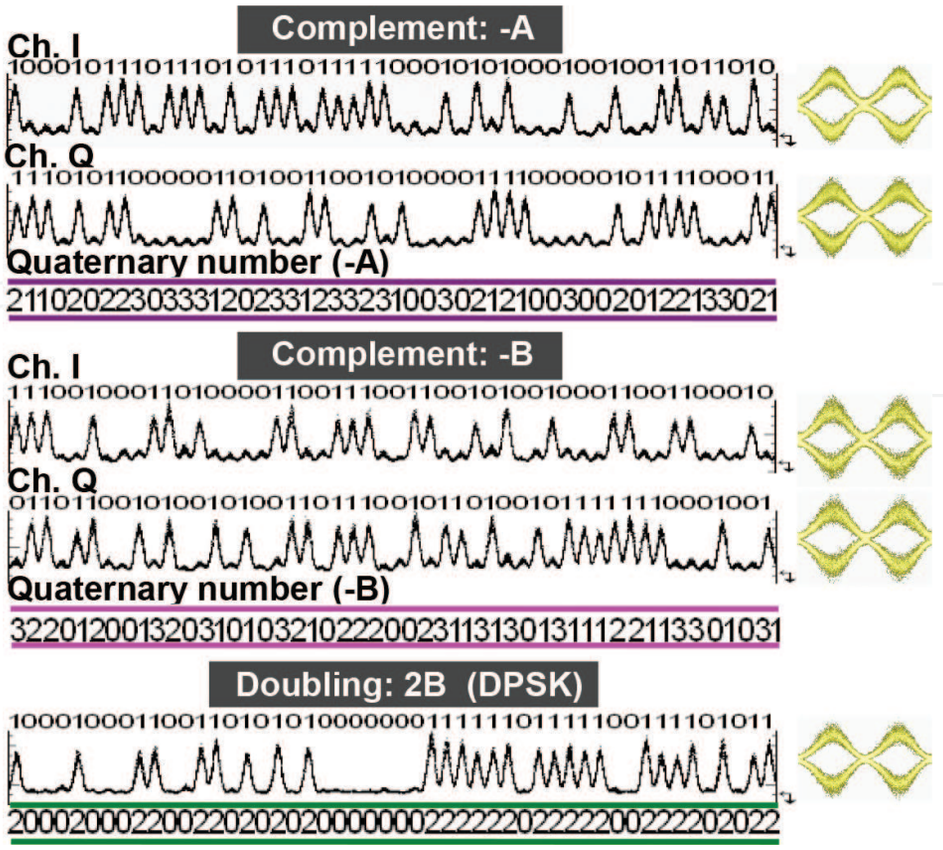

Figure 7. Demodulated waveforms and balanced eyes for 50-Gbaud quaternary complement and doubling using 100-Gbit/s (D)QPSK signals.

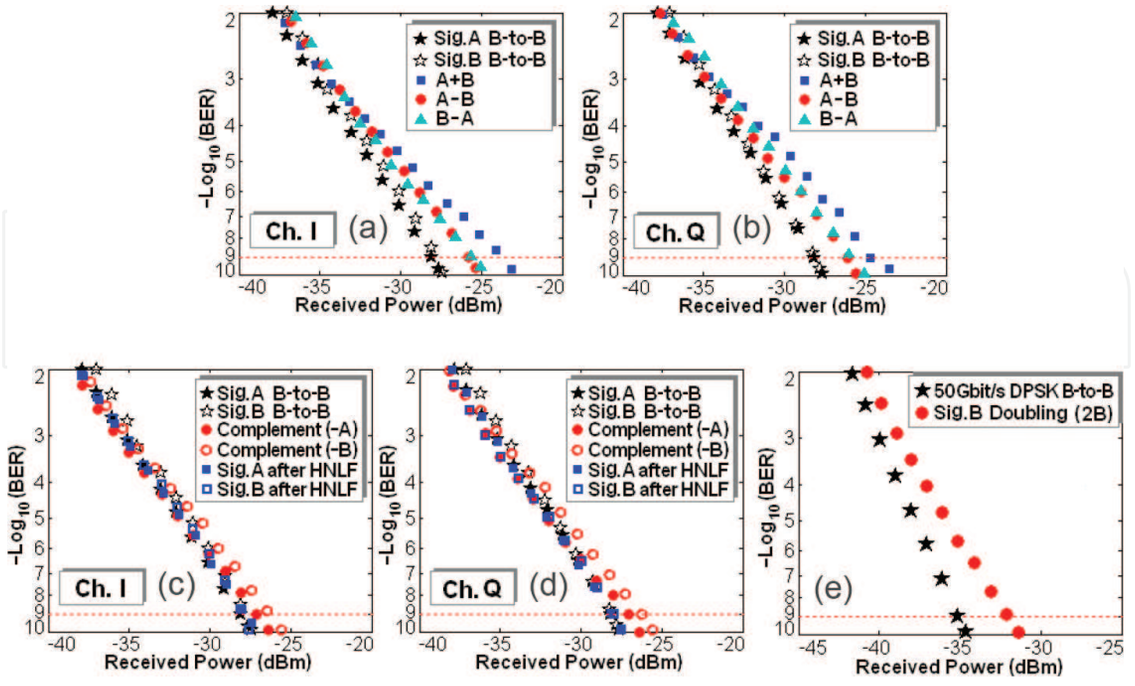

Figure 8. Measured BER curves for input/output signals (A, B), quaternary addition (A+B), dual-directional subtraction (A−B, B−A), complement (−A, −B), and doubling (2B).

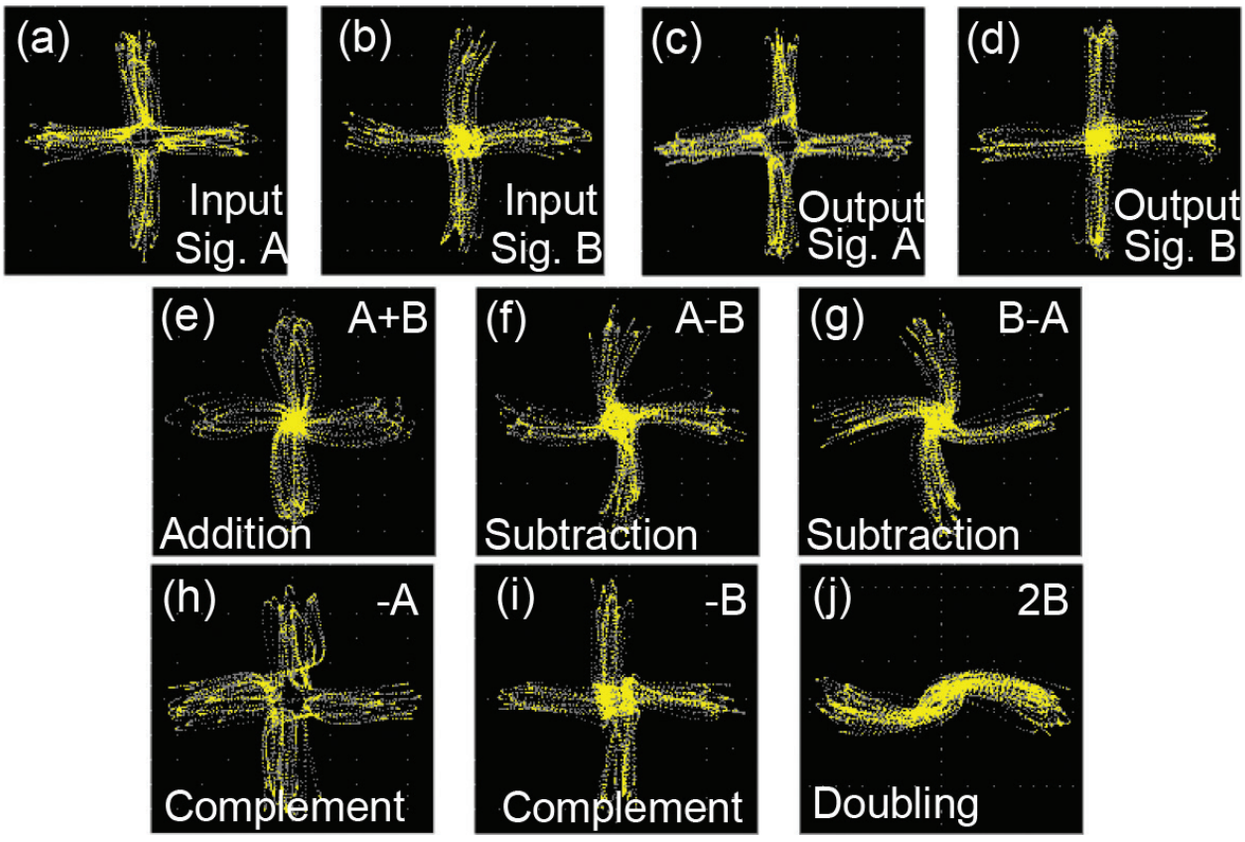

Figure 9. Measured constellations for 50-Gbaud two-input quaternary addition, dual-directional subtraction, complement, and doubling using 100-Gbit/s (D)QPSK signals.

4. Graphene-enhanced optical nonlinearity for M-ary optical computing

Graphene as a purely two-dimensional material with only one-carbon-atom thickness has received great interest since it features many interesting and useful electrical, optical, chemical, and mechanical properties [92, 93]. Over the last decade, many remarkable optical properties of graphene have been discovered, such as self-luminosity, tunable optical absorption, strong nonlinearity, saturable absorption, etc. [94–96]. Recently, optical nonlinearities have been observed in graphene in various configurations, e.g., slow-light graphene-silicon photonic crystal waveguide [97], graphene optically deposited onto fiber ferrules [98], and graphene based on microfiber [99]. The large absorption and Pauli blocking effect in graphene, together with the ultrafast carrier dynamics and strong optical nonlinearity with a fast response time, make graphene-based photonic devices suitable for performing efficient nonlinear functions. Very recently, an experimental observation of FWM-based wavelength conversion of a 10-Gb/s non-return-to-zero (NRZ) signal was reported [100]. In this section, we introduce our recent progress in optical M-ary computing functions using a graphene-assisted nonlinear optical device.

Figure 10 illustrates the fabrication process of the graphene-assisted nonlinear optical device. First, a monolayer graphene was grown on a Cu foil by the chemical vapor deposition (CVD) method. Poly(methyl methacrylate) (PMMA) film was next spin coated on the surface

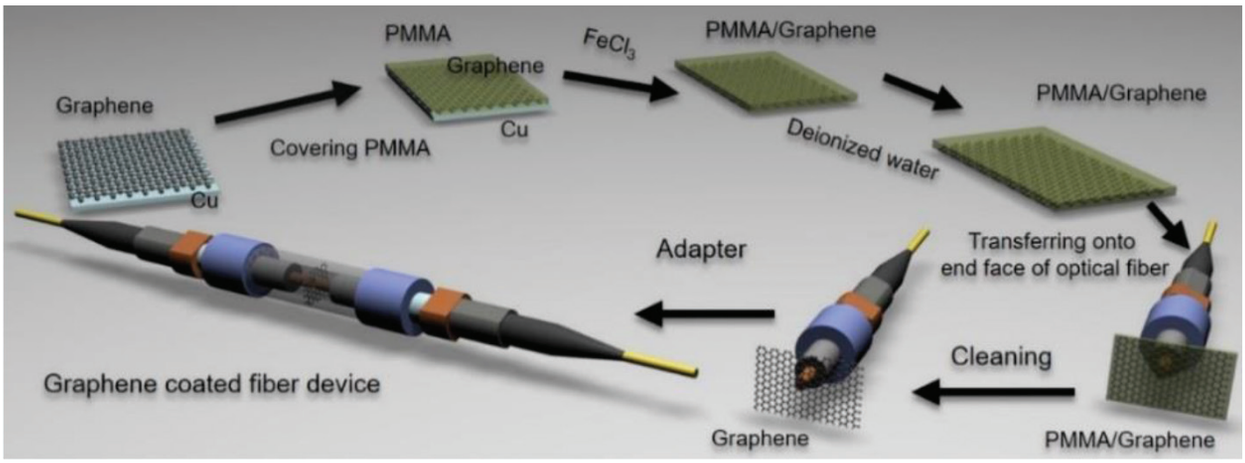

Figure 10. Fabrication process of the graphene-assisted nonlinear optical device.

of the graphene-deposited Cu foil, and the Cu foil was etched away with 1 M $FeCl_3$ solution. The resultant PMMA/graphene film (5 mm × 5 mm) was then washed in deionized water several times and transferred to deionized water solution or Si/SiO_2 substrate. Then, the floating PMMA/graphene sheet was mechanically transferred onto the fiber pigtail cross section and dried in a cabinet. After drying at room temperature for about 24 hours, the carbon atoms could be self-assembled onto the fiber end facet. The PMMA layer was finally removed by boiling acetone. By connecting this graphene-on-fiber component with another clean and dry fiber connector, the nonlinear optical device was thereby constructed for nonlinear optical signal processing applications.

Figure 11(a) depicts the optical microscope (OM) image of the grown graphene film transferred on a 300-nm SiO_2/Si substrate. **Figure 11(b)** shows a scanning electron microscopy (SEM) image of the graphene sheet transferred on silicon-on-insulator (SOI). One can clearly see the evidence of the uniformity of the graphene. The Raman spectrum of the graphene, as displayed in **Figure 11(c)**, shows a weak D peak and a strong 2D peak. The D to G peak intensity ratio is ~0.08, which indicates that the graphene formed on a SiO_2/Si substrate was almost defect-free.

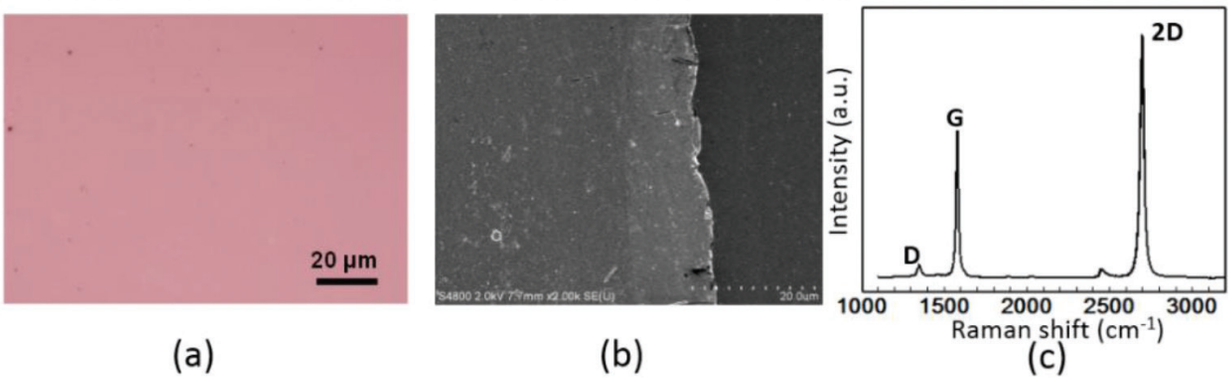

Figure 11. (a) Optical microscope (OM) image of graphene transferred on a SiO_2/Si substrate. (b) SEM image of graphene transferred on silicon-on-insulator (SOI). (c) Typical Raman spectrum of single-layer graphene on a SiO_2/Si substrate (excitation wavelength: 532 nm).

http://dx.doi.org/10.5772/67351

We first examine the wavelength conversion of the graphene-assisted nonlinear optical device. **Figure 12(a)** shows a typical output FWM spectrum obtained after the CVD single-layer graphene-coated fiber device. In the experiment, the signal wavelength is fixed at 1550.12 nm. A newly converted idler at 1546.88 nm is generated when the pump is set to be 1548.49 nm. We also measure the output spectrum without graphene for reference under the same experimental conditions. As clearly shown in the inset of **Figure 12(a)**, the power of converted idler without graphene is observed to be ~5.5 dB lower than the one with graphene. That is, under the same experimental conditions, the converted idler without graphene is ~71.9% lower than the one with graphene. Hence, the degenerate FWM in graphene contributes more in the wavelength conversion process. The insets of **Figure 12(a)** also depict measured QPSK constellations of the converted idler and the input signal. We also present a comparison of the FWM conversion efficiency as a function of the pump power with and without graphene. As shown in **Figure 12(b)**, the pump wavelength is fixed at λ_{pump} = 1548.49 nm and the signal is λ_{signal} = 1550.12 nm. One can clearly see that the conversion efficiency increases with the pump power. When the pump power varies from 23 dBm to 33 dBm, the enhanced FWM conversion efficiency by graphene changes from 4.7 dB to 7.5 dB.

Figure 13(a) plots the converted idler wavelength as a function of the pump wavelength when the pump power is fixed at 31 dBm. A linear wavelength relationship between the converted idler and pump is observed. The measured FWM conversion efficiency of tunable wavelength conversion with and without graphene is shown in **Figure 13(b)**. The signal wavelength is fixed at 1550.12 nm and the pump wavelength is tuned from 1547 to 1553 nm. When using graphene-coated fiber device, the conversion efficiency varies about 1.7 dB within a ~6 nm wavelength range. By comparing the measured pump wavelength-dependent conversion efficiency with and without graphene, one can clearly see that the FWM conversion efficiency with graphene is enhanced more than 5 dB within the tuning range of pump wavelength.

To characterize the performance of QPSK wavelength conversion, we further measure the BER curve as a function of the received observed OSNR for B-to-B signal and converted idler.

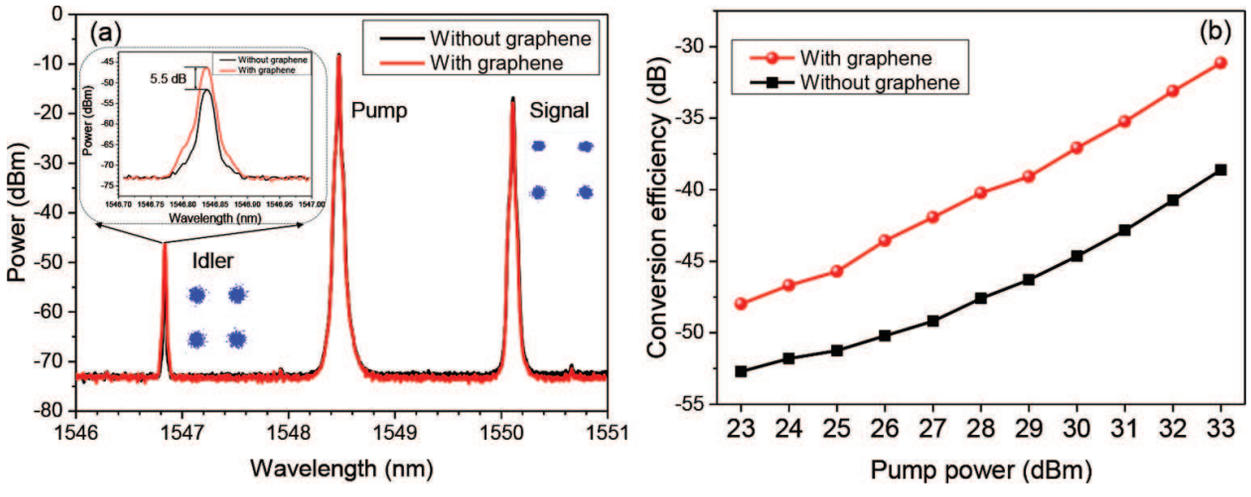

Figure 12. (a) Measured FWM spectra with (circle) and without (square) graphene. (b) Measured conversion efficiency of FWM with and without graphene when pump power is tuned from 23 to 33 dBm.

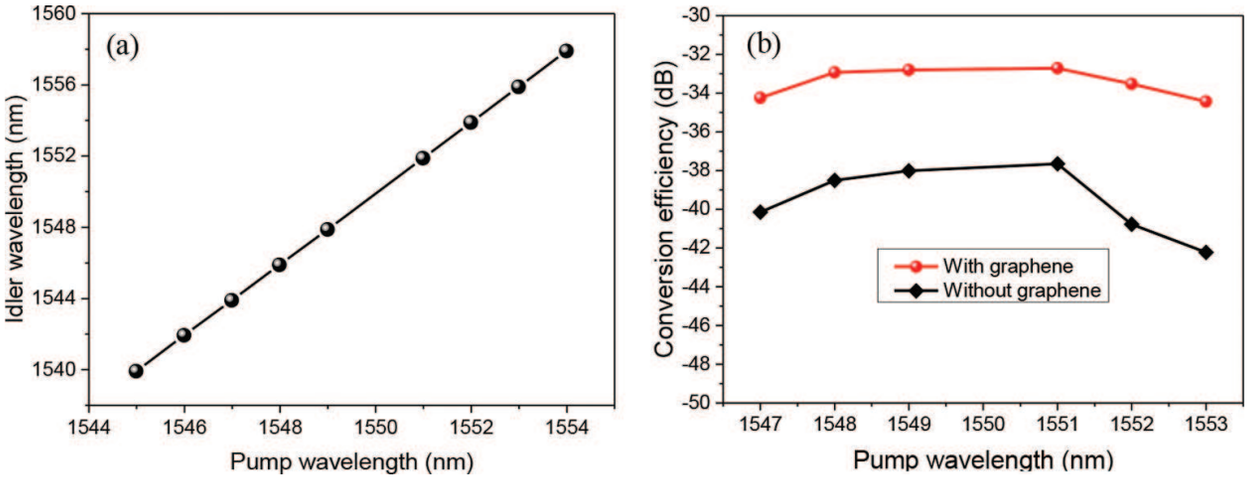

Figure 13. (a) Converted idler wavelength versus pump wavelength. (b) Measured FWM conversion efficiency with and without graphene when pump wavelength is tuned from 1547 to 1553 nm. Pump power: 31 dBm.

Figure 14 plots measured BER performance for tunable QPSK wavelength conversion with the converted idler generated at 1546.88, 1539.92, and 1557.90 nm, respectively. The measured conversion efficiencies for converted idlers at 1546.88, 1539.92, and 1557.90 nm are −36.2, −48.2, and −39.8 dB, respectively. As shown in **Figure 14**, the observed OSNR penalty is around 1 dB at a BER of 1×10^{-3} (7% forward error correction (FEC) threshold) for QPSK wavelength conversion with the converted idler at 1546.88 nm. The received OSNR penalties of ~2.2 dB at a BER of 1×10^{-3} are observed for converted idlers at 1539.92 and 1557.90 nm. The increased OSNR penalty is mainly due to the reduced conversion efficiency for converted idlers at 1539.92 and 1557.90 nm. The right insets of **Figure 14** depict corresponding constellations of the B-to-B signals and converted idlers. The obtained results shown in **Figures 11–14** imply favorable performance achieved for tunable wavelength conversion of QPSK signal using a fiber pigtail cross section coated with a single-layer graphene.

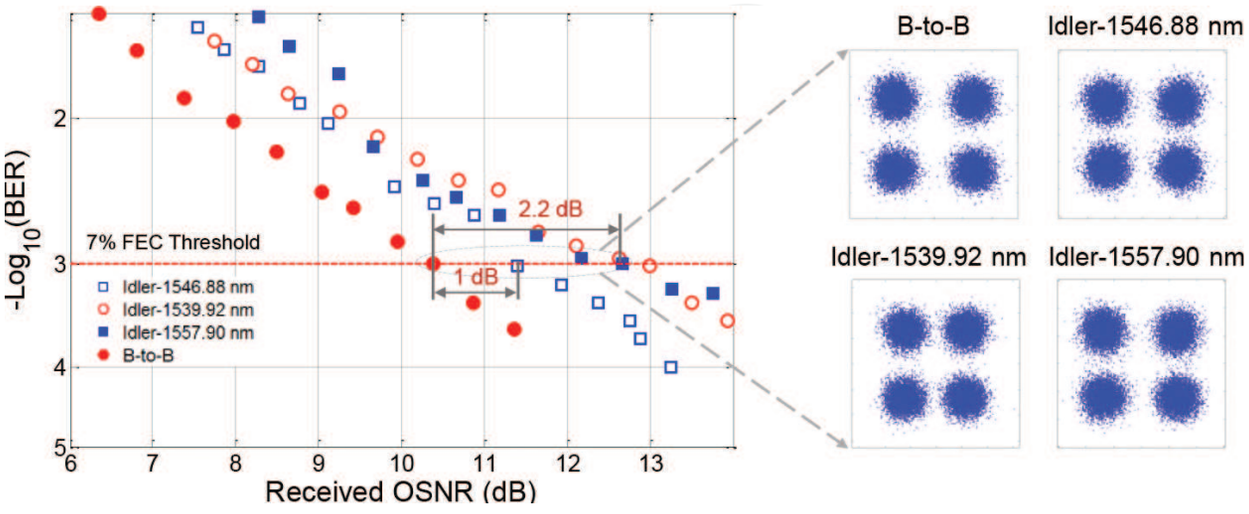

Figure 14. Measured BER versus received OSNR for wavelength conversion of QPSK signal. Insets show constellations of QPSK.

We then show the results of optical computing based on the fabricated graphene-assisted nonlinear optical device. **Figure 15** illustrates the concept and principle of two-input hybrid quaternary arithmetic functions. From the constellation in the complex plane (**Figure 15(a)**), it is clear that one can use four-phase levels (π/4, 3π/4, 5π/4, 7π/4) of (D)QPSK to represent quaternary base numbers (0, 1, 2, 3). To implement two-input hybrid quaternary arithmetic functions, the aforementioned graphene-assisted nonlinear optical device is employed. Two-input quaternary numbers (A, B) are coupled into the nonlinear device, and then two converted idlers (idler 1, idler 2) are simultaneously generated by two degenerate FWM processes. **Figure 15(b)** illustrates the degenerate FWM process. We derive the electrical field (E) and optical phase (Φ) relationships of two degenerate FWM processes under the pump non-depletion approximation expressed as

$$E_{i1} \propto E_A \cdot E_A \cdot E_B^*, \quad \Phi_{i1} = \Phi_A + \Phi_A - \Phi_B \tag{7}$$

$$E_{i2} \propto E_B \cdot E_B \cdot E_A^*, \quad \Phi_{i2} = \Phi_B + \Phi_B - \Phi_A \tag{8}$$

where the subscripts A, B, i1, and i2 denote input signal A, signal B, converted idler 1, and idler 2, respectively. Owing to the phase wrap characteristic with a periodicity of 2π, it is implied from the linear phase relationships in Eqs. (7) and (8) that idler 1 and idler 2 carry out modulo 4 operations of hybrid quaternary arithmetic functions of doubling and subtraction (2A−B, 2B−A).

Figure 16 depicts measured typical spectrum obtained after the CVD single-layer graphene-coated fiber device. Two 10-Gbaud NRZ-(D)QPSK signals at 1550.10 (A) and 1553.60 nm (B) are employed as two inputs. The power of two input signals (A, B) is about 32 dBm. The conversion efficiency is measured to be around −36 dB. One can clearly see that two converted idlers are obtained by two degenerate FWM processes with idler 1 at 1546.60 nm (2A−B) and idler 2 at 1557.20 nm (2B−A). The resolution of the measured spectrum is set to 0.02 nm. The steps in the measured spectrum are actually the modulation sidebands of two NRZ-(D)QPSK carrying signals. In order to verify the hybrid quaternary arithmetic functions, we measure the phase of symbol sequence for two input signals and two converted idlers, as shown in **Figure 17**. By carefully comparing the quaternary base numbers for two input signals and two converted idlers, one can confirm the successful implementation of two-input hybrid quaternary arithmetic functions of 2A−B and 2B−A.

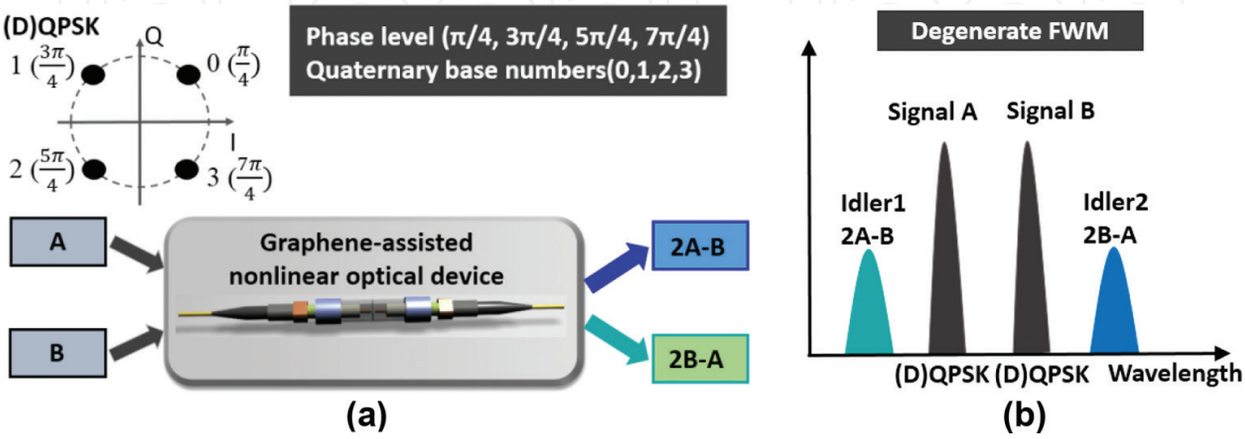

Figure 15. (a) Concept and (b) principle of hybrid quaternary arithmetic functions (2A−B, 2B−A) using degenerate FWM and (D)QPSK signals.

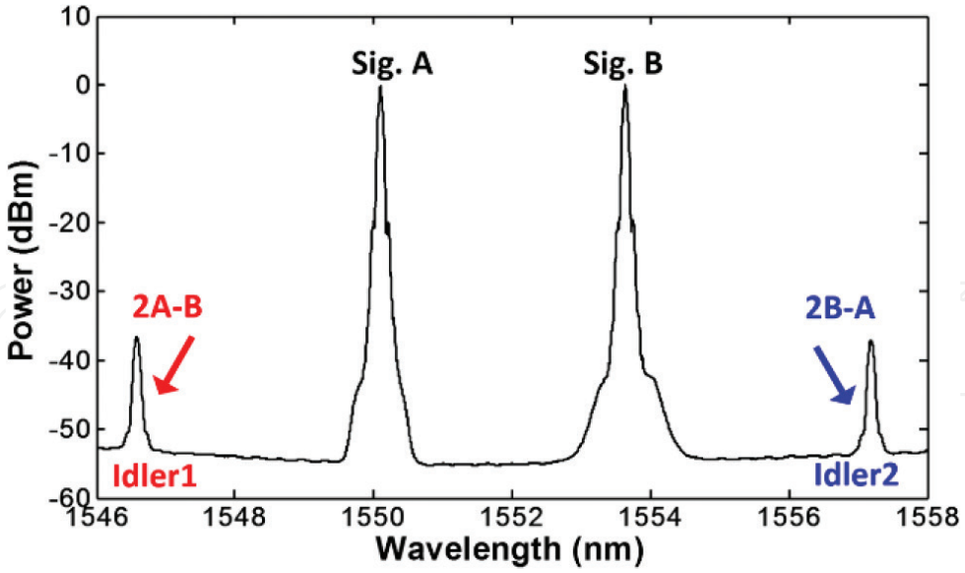

Figure 16. Measured spectrum for 10-Gbaud two-input hybrid quaternary arithmetic functions.

We further investigate the BER performance for the proposed optical two-input hybrid quaternary arithmetic functions. The OSNR penalties at a BER of 2×10^{-3} for hybrid quaternary arithmetic functions are measured to be about 7.4 dB for 2A−B and 7.0 dB for 2B−A. The insets in **Figure 18(a)** show constellations of the last point of the BER curves of output Sig. B and 2A−B. The constellation of Sig. B is measured under an OSNR of 12.6 dB, while the constellation of 2A−B is observed under an OSNR of 19.6 dB. To clearly show the differences between these two constellations, we also assess the EVM of these two constellations, i.e., EVM = 27.61% for output Sig. B and EVM = 30.09% for output 2A−B. The significant performance degradations for the two-input hybrid quaternary arithmetic functions (2A−B, 2B−A) might

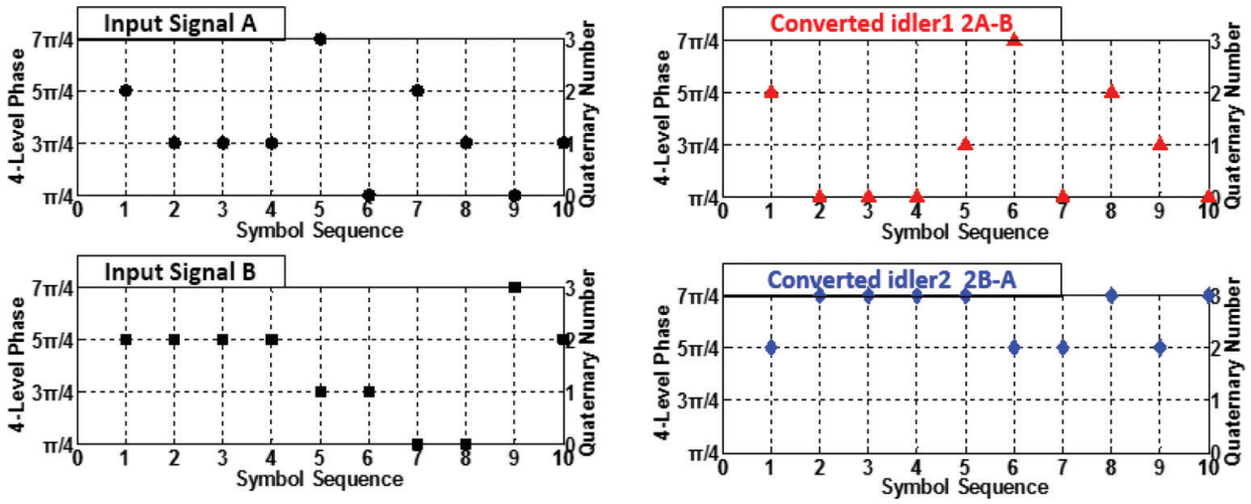

Figure 17. Measured phase of symbol sequence with coherent detection for 10-Gbaud two-input hybrid quaternary arithmetic functions.

http://dx.doi.org/10.5772/67351

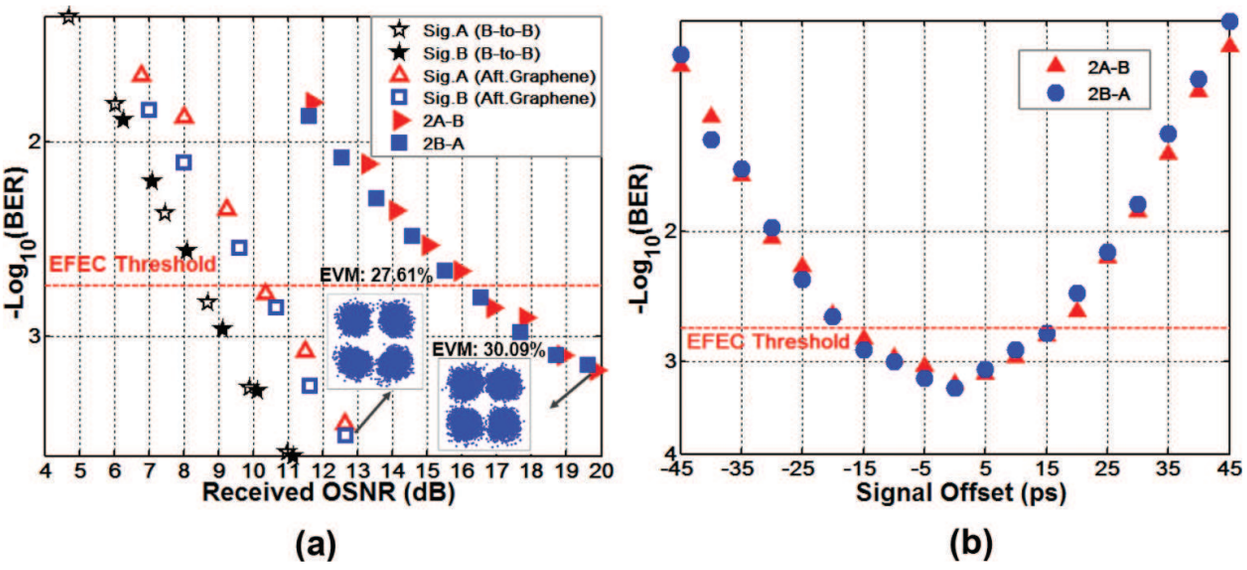

Figure 18. Measured BER curves for two-input hybrid quaternary arithmetic functions of 2A−B and 2B−A; (b) BER versus signal offset.

be ascribed to the relatively low conversion efficiency for two converted idlers at 1546.60 nm and 1557.20 nm and accumulated distortions transferred from two input signals (A, B). It is possible to further enhance the conversion efficiency by appropriately increasing the number of graphene layers employed in the experiment. **Figure 18(b)** depicts the BER performance as a function of the relative time offset between two signals (signal offset) under an OSNR of ~20 dB. It is found that the BER is kept below enhanced forward error correction (EFEC) threshold when the signal offset/symbol time is within 15 ps, which indicates a favorable tolerance to the signal offset.

We also propose an approach to performing three-input optical addition and subtraction of quaternary base numbers using multiple nondegenerate FWM processes based on graphene-assisted device.

Figure 19 illustrates the concept and working principle of the proposed graphene-assisted three-input high-base optical computing. Three input (D)QPSK signals (A, B, C) are launched into the nonlinear device, in which three converted idlers (idler 1, idler 2, idler 3) are simultaneously generated by three nondegenerate FWM processes. Quaternary hybrid addition and subtraction of A+B−C, A+C−B, and B+C−A are obtained simultaneously.

In the experiment, the wavelengths of three input signals A, B, and C are fixed at 1548.52, 1550.12, and 1552.52 nm, respectively. **Figure 20** depicts measured typical optical spectrum obtained after the single-layer graphene-coated fiber device. One can clearly see that three converted idlers are generated by three nondegenerate FWM processes with idler 1 at 1546.13 nm (A+B−C), idler 2 at 1550.92 nm (A+C−B), and idler 3 at 1554.13 nm (B+C−A), respectively. The conversion efficiencies of three nondegenerate FWM processes are measured to be larger than −34 dB. In order to verify the quaternary optical computing functions, we measure the phase of symbol sequence for three input signals and three converted idlers, as shown in

Figure 21. By carefully comparing the quaternary base numbers for three input signals and three converted idlers, one can confirm the successful implementation of graphene-assisted three-input quaternary optical computing (i.e., quaternary hybrid addition and subtraction) functions of A+B−C, A+C−B, and A+C−B.

To characterize the performance of the proposed graphene-assisted three-input high-base optical computing functions, we further measure the BER curves as a function of the received OSNR for B-to-B signals and three converted idlers. **Figure 22** depicts measured BER curves for 10-Gbaud three-input quaternary hybrid addition and subtraction of A+B−C, A+C−B, and B+C−A. As shown in **Figure 22**, the observed OSNR penalties of three-input quaternary hybrid addition and subtraction are accessed to be less than 7 dB at a BER of 2×10^{-3} (7% EFEC threshold). The increased OSNR penalties might be mainly due to the relatively low conversion efficiency for converted idlers and accumulated distortions transferred from three input signals (A, B, C). The insets in **Figure 22** depict corresponding constellations of the B-to-B signals and converted idlers. The BER curves and constellations of three output signals (A, B, C) after graphene are also shown in **Figure 22** for reference.

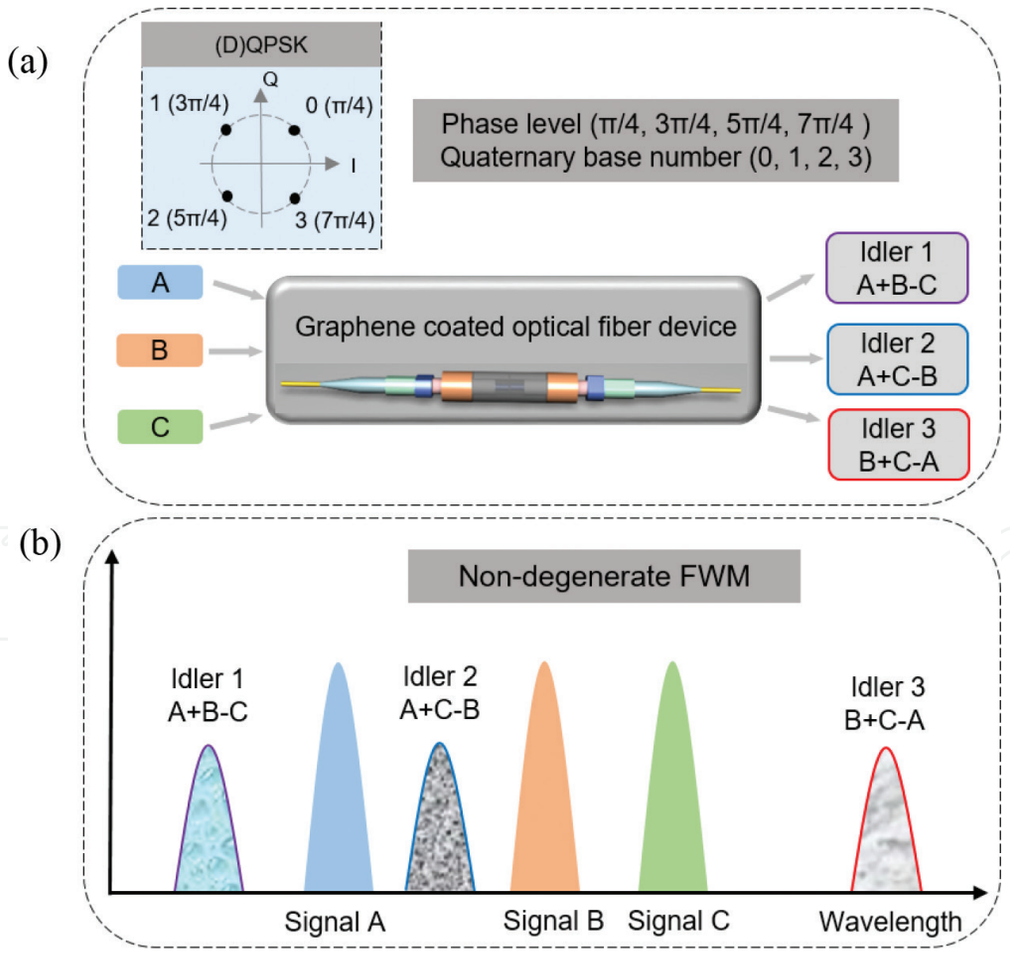

Figure 19. (a) Concept and (b) principle of graphene-assisted three-input (A, B, C) quaternary hybrid addition and subtraction (A+B−C, A+C−B, B+C−A) using nondegenerate FWM and (D)QPSK signals.

http://dx.doi.org/10.5772/67351

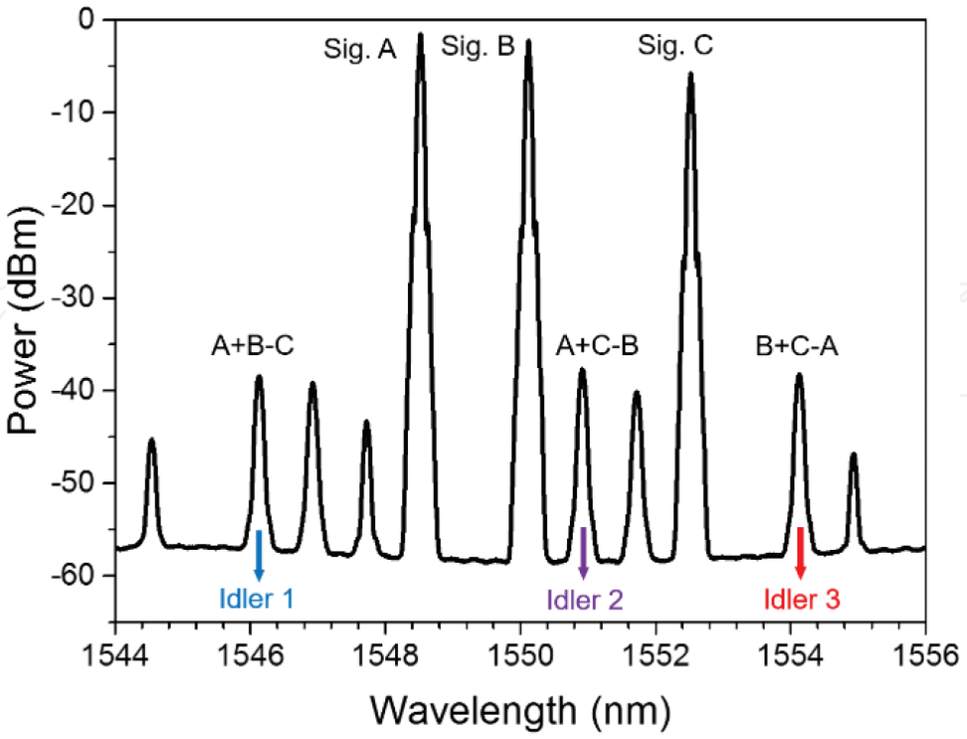

Figure 20. Measured spectrum for 10-Gbaud three-input quaternary hybrid addition and subtraction.

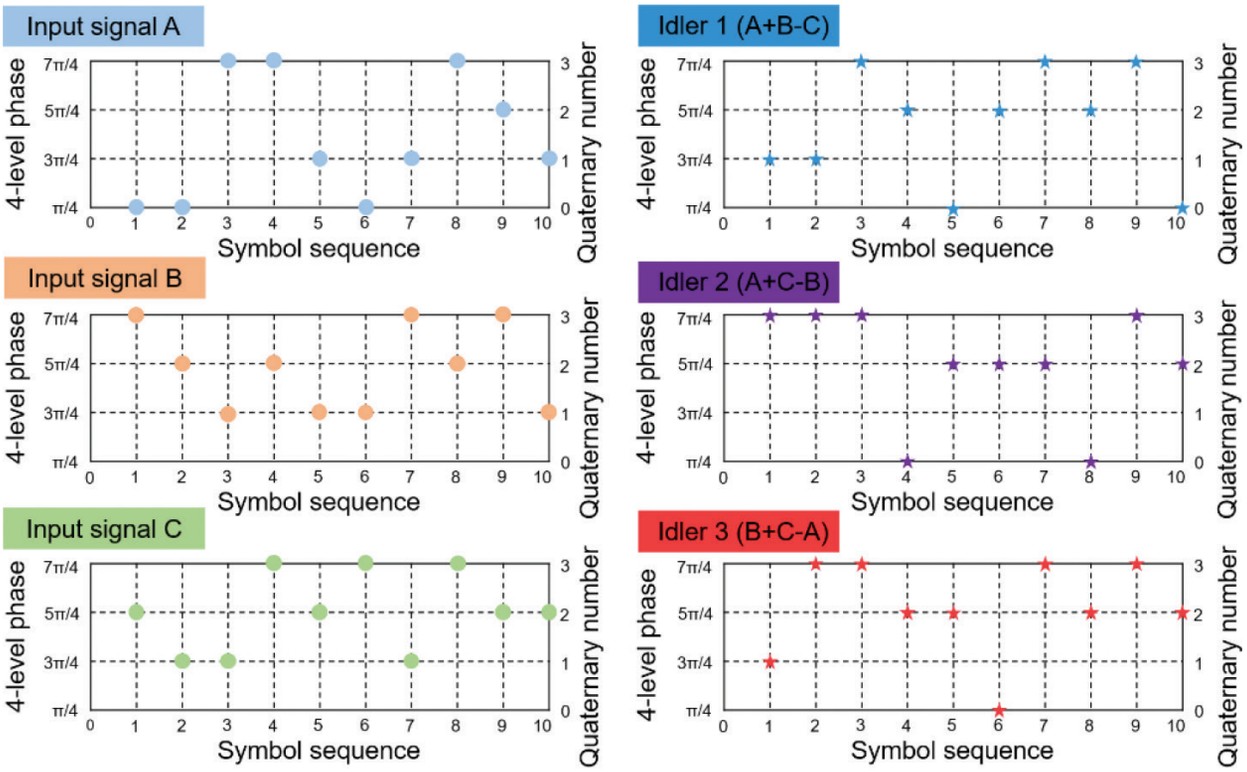

Figure 21. Measured phase of symbol sequence by coherent detection for 10-Gbaud three-input quaternary hybrid addition and subtraction.

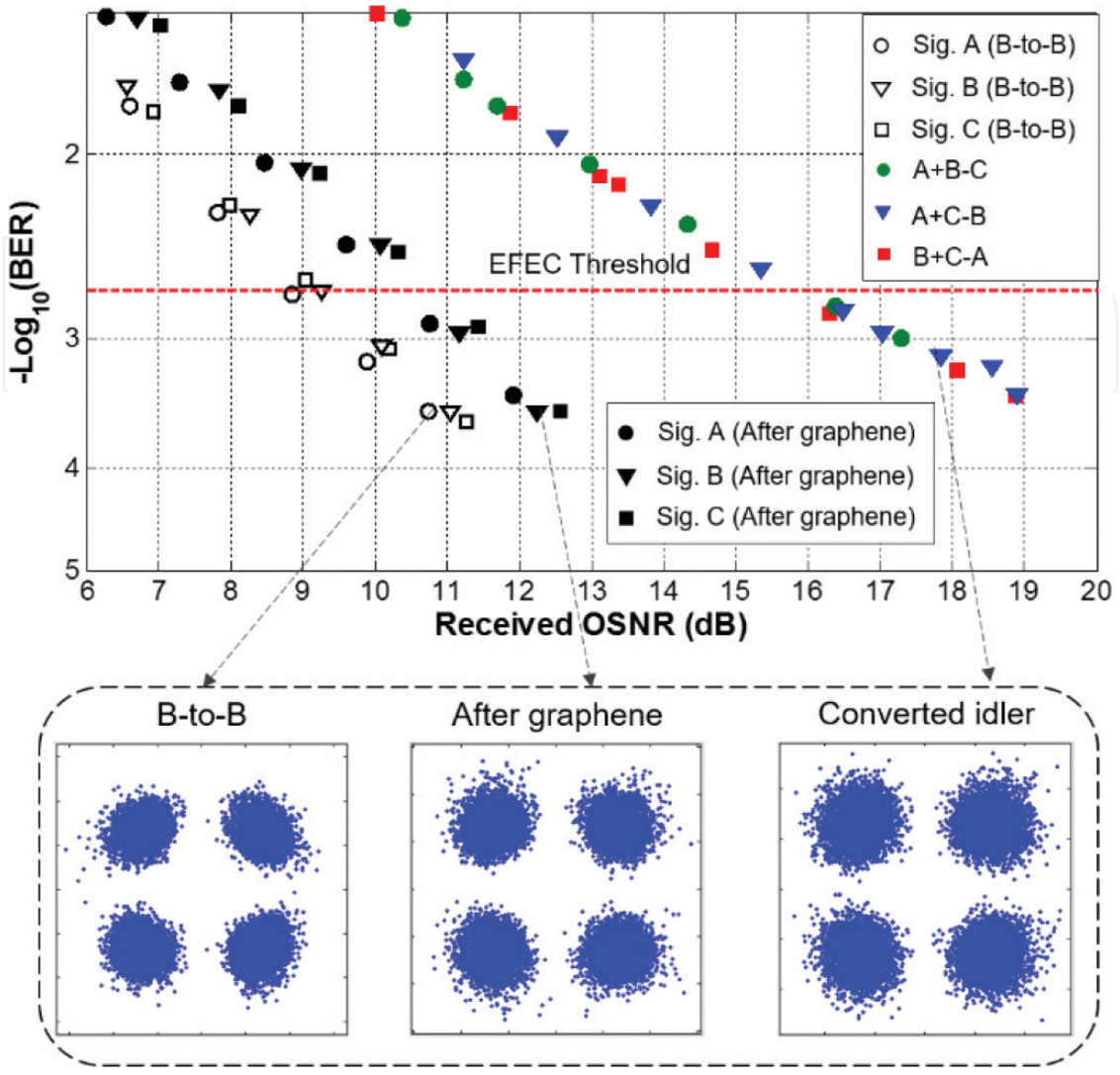

Figure 22. Measured BER curves for 10-Gbaud three-input quaternary hybrid addition and subtraction of A+B−C, A−C−B, and B+C−A. Insets show constellations of (D)QPSK signals.

5. On-chip M-ary optical computing

Silicon photonics has become one of the most promising photonic integration platforms for its ultrahigh level of integration, low power consumption, and CMOS compatibility. In addition, nonlinear interaction will also be enhanced in silicon waveguides due to its tight light confinement. Thus, SOI is also considered to be a favorable nonlinear optics platform. To minimize the footprint of the computing building block and lower the power consumption, we demonstrate on-chip M-ary optical computing by adopting silicon photonics technology.

We first experimentally demonstrate all-optical two-input (A, B) optical quaternary doubling/subtraction (2A−B, 2B−A) using a silicon waveguide. The silicon waveguide used in the experiment is shown in **Figure 23**.

Figure 23. Photomicrograph of the silicon waveguide.

Figure 24 shows the measured symbol sequence for two-input optical quaternary hybrid doubling/subtraction. It can be confirmed from **Figure 24** that simultaneous quaternary hybrid doubling/subtraction (2A−B, 2B−A) are successfully implemented using QPSK, degenerate FWM, and coherent detection.

We also experimentally demonstrate three-input (A, B, C) optical quaternary addition/subtraction (A+C−B, A+B−C, B+C−A) using such a silicon waveguide. **Figure 25** shows the measured symbol sequence for three-input optical quaternary addition/subtraction.

It is relatively difficult to experimentally demonstrate higher-order computing using a pure silicon waveguide due to the large OSNR penalty. Thus, we simulate hexadecimal optical computing using nonlinear interactions in a silicon-organic hybrid slot waveguide [101]. **Figure 26(a)** shows the structure of a silicon-organic hybrid slot waveguide. It features a

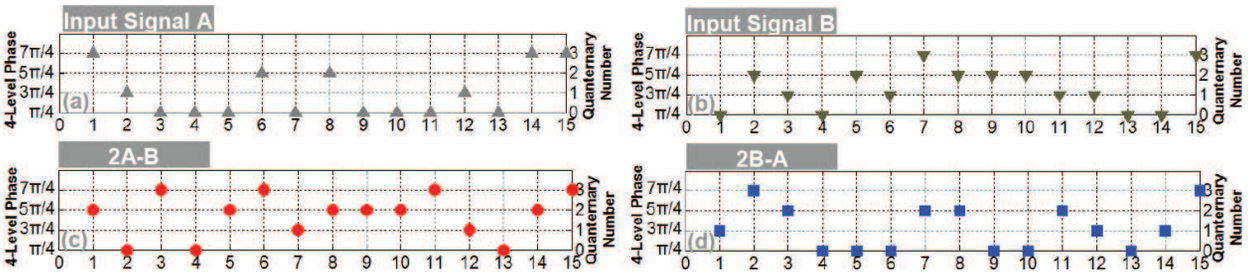

Figure 24. Measured symbol sequence for two-input optical quaternary addition/subtraction (2A−B, 2B−A).

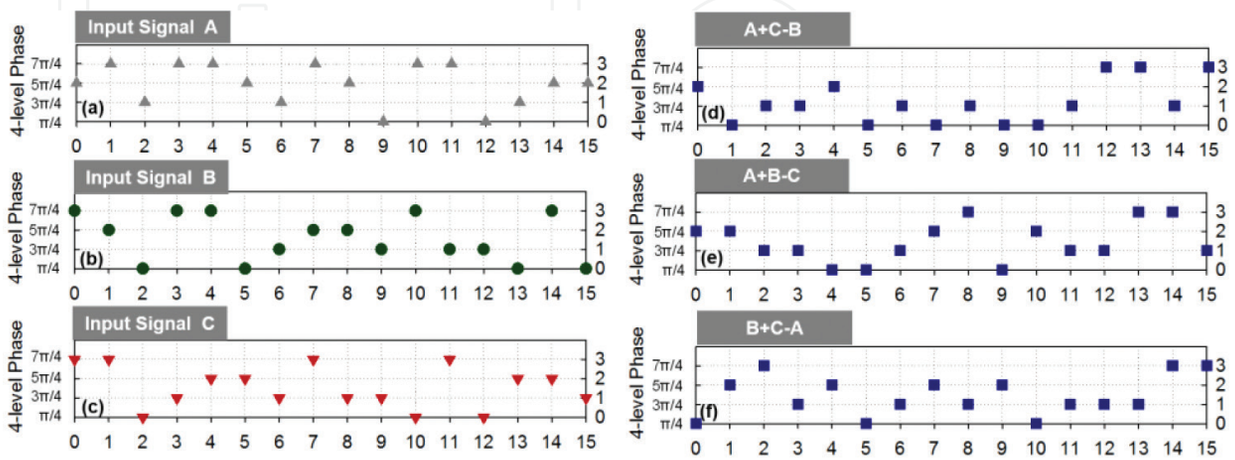

Figure 25. Measured symbol sequence for (a)–(c) three-input optical quaternary signal and their (c)–(e) addition/subtraction.

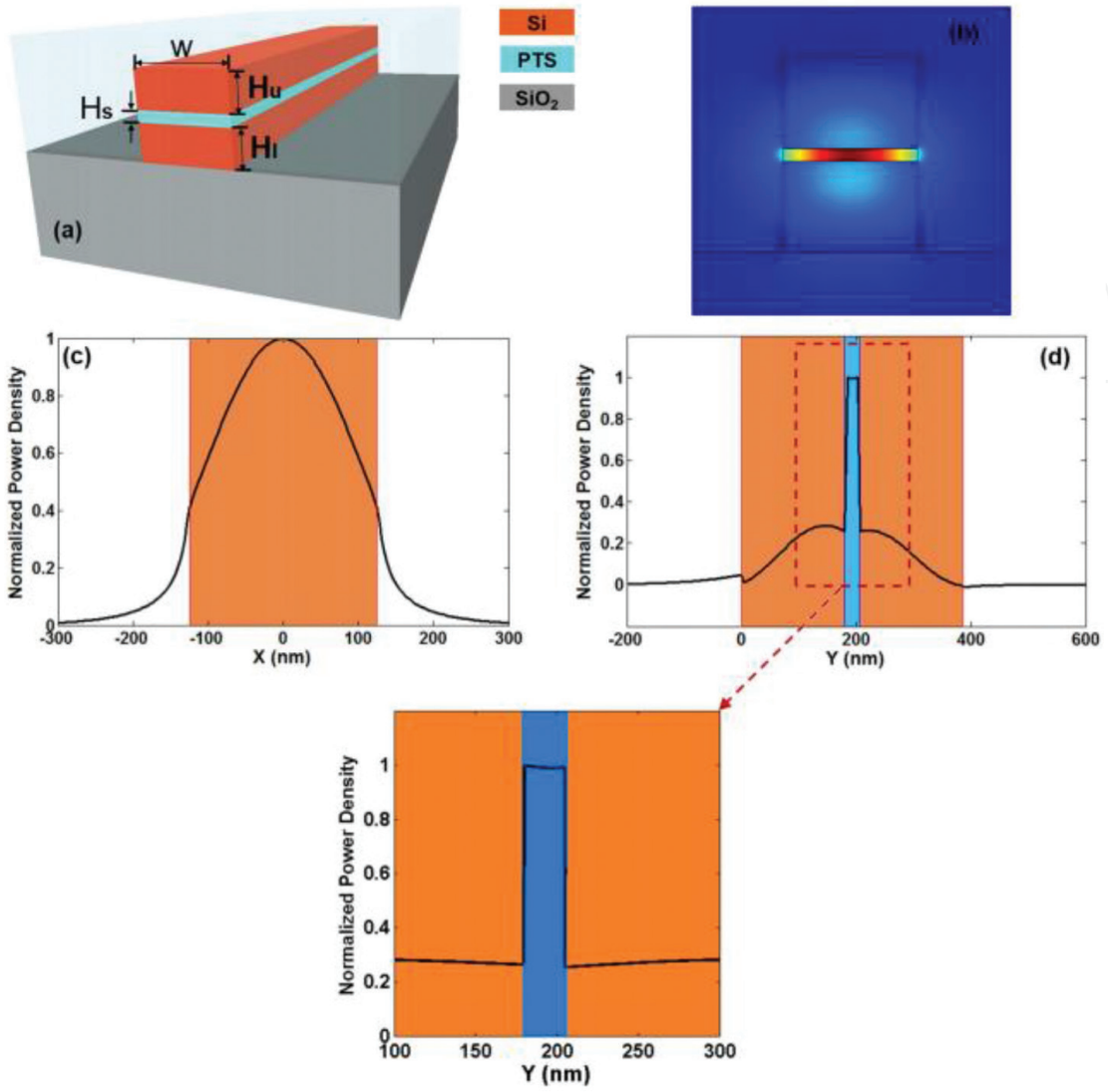

Figure 26. (a) 3D structure, (b) mode distribution, (c) and (d) normalized power density along x and y directions of a silicon-organic hybrid slot waveguide.

sandwich structure with a low-refractive-index PTS [polymer poly (bis para-toluene sulfonate)] layer surrounded by two high refractive index silicon layers. The TM mode profile and its power density along x/y directions are depicted in **Figure 26(b)–(d)**. Tight light confinement is observed in the nanoscale nonlinear organic slot region, which offers high nonlinearity and instantaneous Kerr response. We assess the effective mode area and nonlinearity to be 7.7×10^{-14} m^2 and 5500 $w^{-1}m^{-1}$, which can potentially facilitate efficient optical signal processing (e.g., hexadecimal addition/subtraction).

Figure 27 depicts simulation results for three-input multicasted 40-Gbaud (160-Gbit/s) hexadecimal addition/subtraction. Twenty symbol sequences are plotted in **Figure 27**, which confirms the successful implementation of three-input hexadecimal addition/subtraction (A + B − C, A + C − B, B + C − A, A + B + C, A − B − C, B − A − C). The constellations are also shown in **Figure 28**.

http://dx.doi.org/10.5772/67351

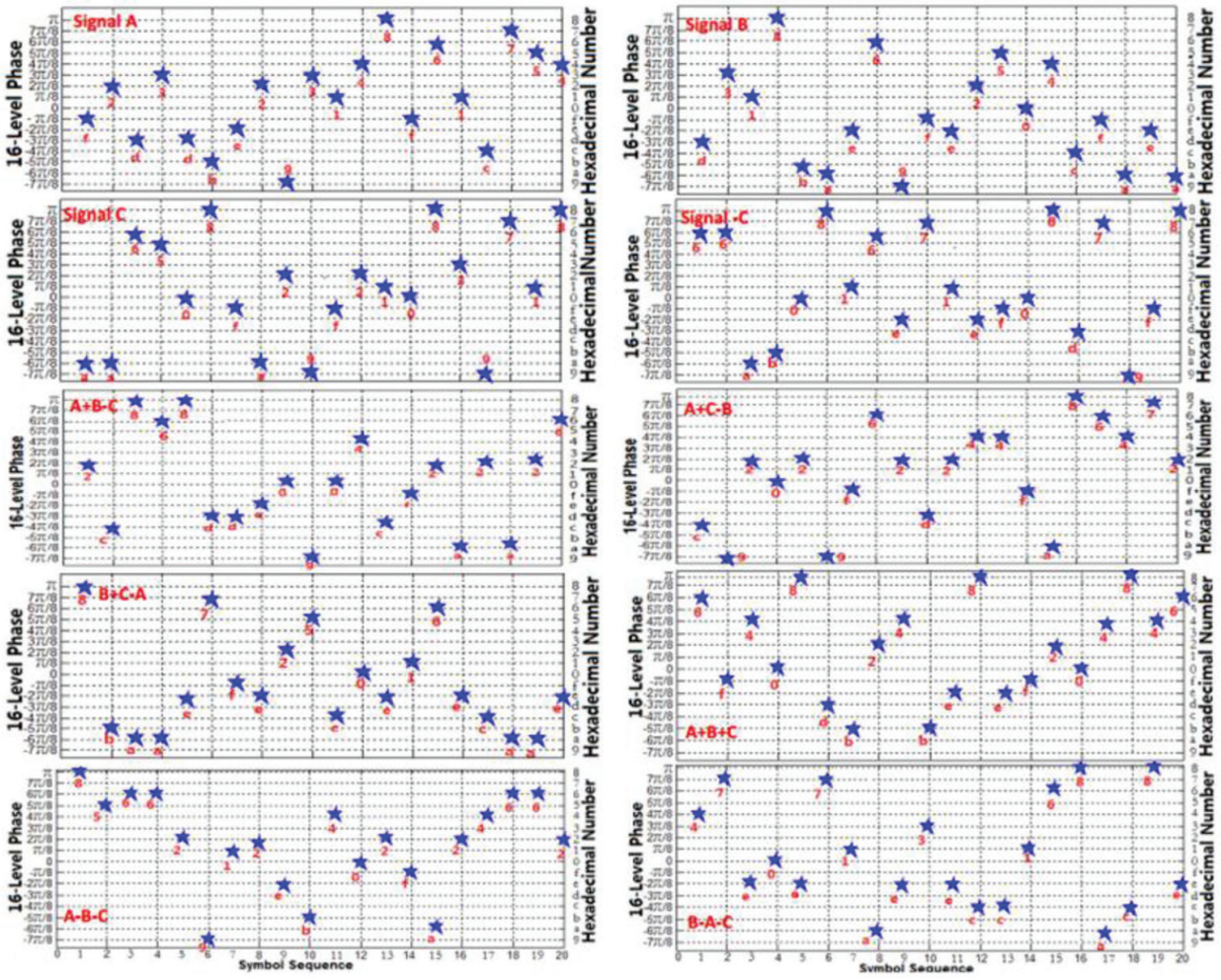

Figure 27. Simulated symbol sequence for three-input multicasted 40-Gbaud (160-Gbit/s) hexadecimal addition/subtraction using a silicon-organic hybrid slot waveguide.

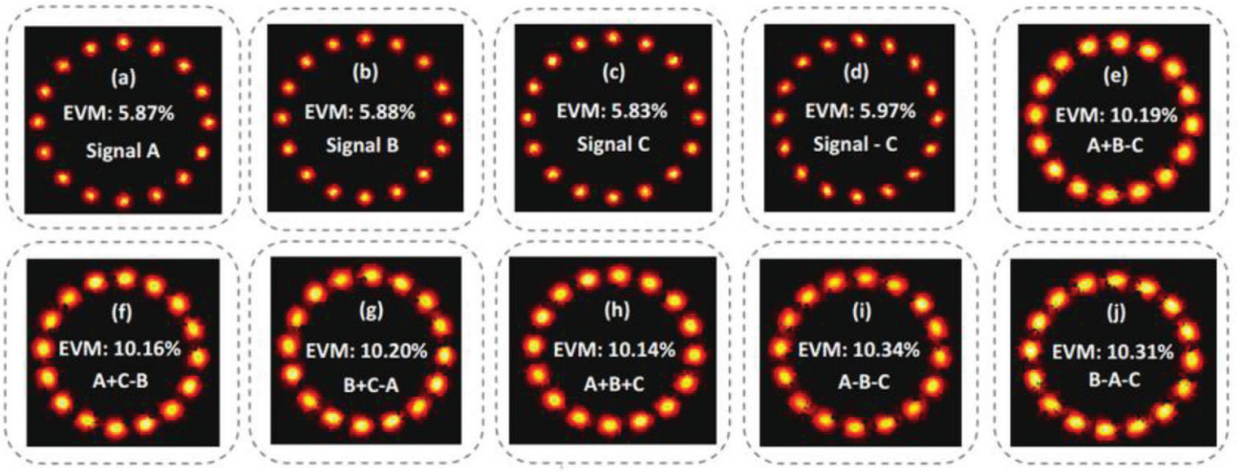

Figure 28. Simulated constellations for three-input multicasted 40-Gbaud (160-Gbit/s) hexadecimal addition/subtraction using a silicon-organic hybrid slot waveguide.

We further investigate the EVM of input signals and output idlers as functions of the OSNR of input signals. The results are shown in **Figure 29(a)** and **(b)**. The EVM penalties are less than 4.5 for hexadecimal addition/subtraction under a 28-dB OSNR. EVM of hexadecimal addition/subtraction as a function of input signal power are shown in **Figure 30**. EVM increases slightly (<0.8 dB) with input signal power <50 mW, which implies a large available dynamic range (~27 dB).

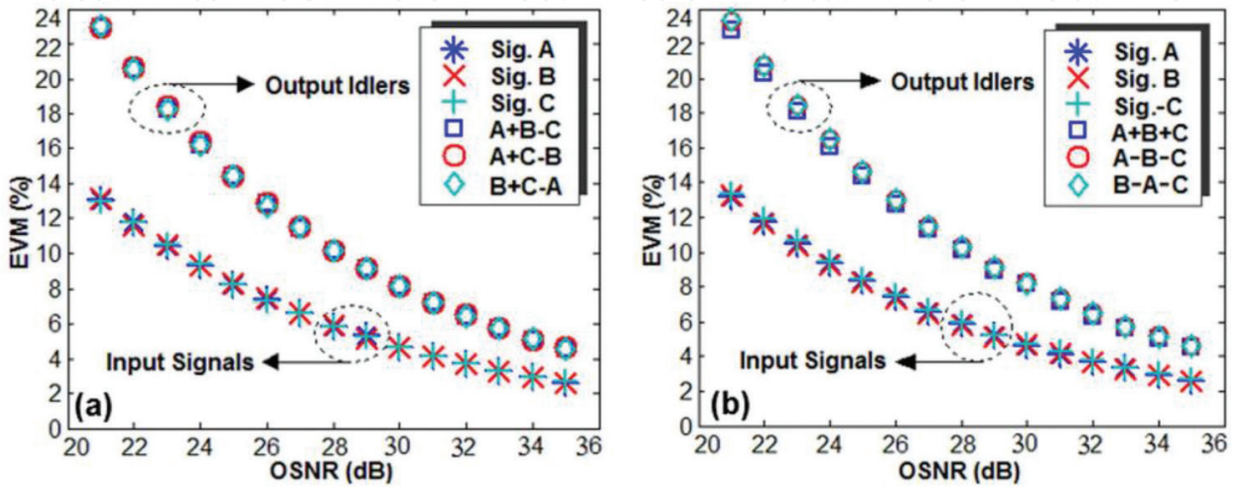

Figure 29. Simulated EVM versus OSNR for 40-Gbaud (160-Gbit/s) hexadecimal addition/subtraction using a silicon-organic hybrid slot waveguide.

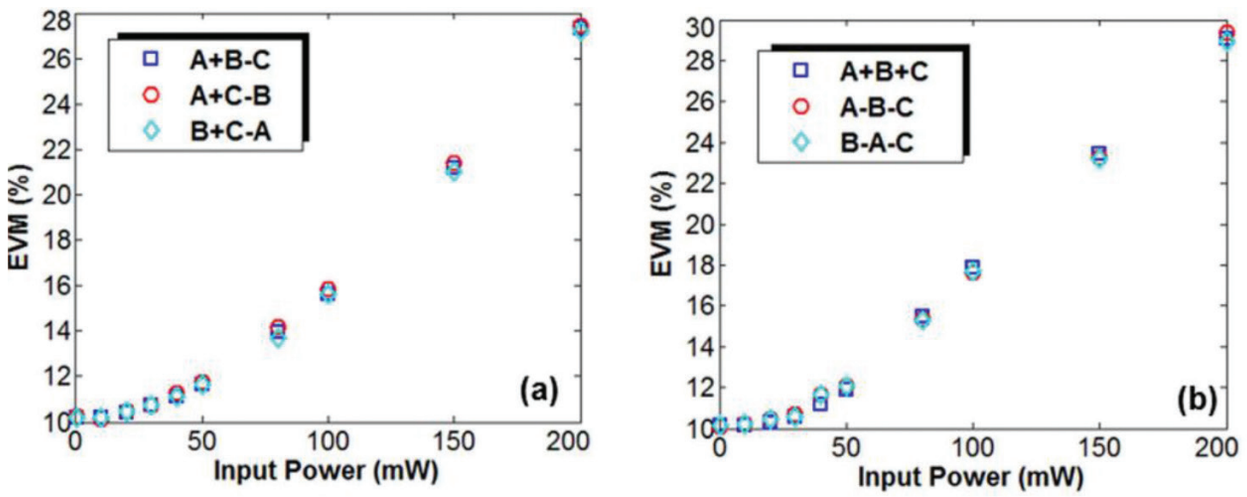

Figure 30. Simulated dynamic range of signal power for 40-Gbaud (160-Gbit/s) hexadecimal addition/subtraction using a silicon-organic hybrid slot waveguide.

6. Conclusion

In this chapter, we have reviewed recent research efforts toward M-ary optical computing by adopting multilevel modulation signals and exploiting optical nonlinearities.

1. M-ary optical computing using HNLF: By adopting 100-Gbit/s two-input (D)QPSK signals (A, B) and exploiting three degenerate FWM processes and three nondegenerate FWM processes in an HNLF, simultaneous 50-Gbaud two-input quaternary addition (A+B), dual-directional subtraction (A−B, B−A), complement (−A, −B), and doubling (2B) have been demonstrated in the experiment.
2. Graphene-enhanced optical nonlinearity for M-ary optical computing: We experimentally demonstrated hybrid two-/three-input quaternary addition/subtraction optical computing in a graphene-assisted nonlinear devices.
3. On-chip M-ary optical computing: To minimize the footprint of the computing building block and lower the power consumption, we demonstrate on-chip M-ary optical computing by adopting silicon photonics technology. We experimentally demonstrated on-chip quaternary addition/subtraction optical computing in a silicon waveguide. On-chip hexadecimal addition/subtraction is also numerically investigated using a silicon-organic hybrid slot waveguide.

Addition and subtraction are considered to be fundamental building blocks of digital signal processing. Optical signal processing technology opens a new world for ultrahigh-speed arithmetic operations. With future improvements, other different optical nonlinearities on various nonlinear optical device platforms would also be employed to flexibly manipulate the amplitude and phase information of advanced multilevel modulation signals. In addition, more complicated computing functionalities can be introduced, which might open diverse interesting applications in robust optical computing operation.

Acknowledgements

This work was supported by the National Program for Support of Top-notch Young Professionals, the National Natural Science Foundation of China (NSFC) under grants 61222502, 11574001, and 11274131, the Program for New Century Excellent Talents in University (NCET-11-0182), the National Basic Research Program of China (973 Program) under grant 2014CB340004, the Wuhan Science and Technology Plan Project under grant 2014070404010201, the Fundamental Research Funds for the Central Universities (HUST) under grants 2012YQ008 and 2013ZZGH003, and the seed project of Wuhan National Laboratory for Optoelectronics (WNLO). The authors thank the Center of Micro-Fabrication and Characterization (CMFC) of WNLO for the support in the manufacturing process of silicon waveguides. The authors also thank the facility support of the Center for Nanoscale Characterization and Devices of WNLO.

Author details

Jian Wang* and Yun Long

*Address all correspondence to: jwang@hust.edu.cn

Wuhan National Laboratory for Optoelectronics, School of Optical and Electronic Information, Huazhong University of Science and Technology, Wuhan, Hubei, China

References

[1] I. Kaminow, T. Li, and A. E. Willner, Optical Fiber Telecommunications VB: Systems and Networks, Elsevier (2010).

[2] P. P. Mitra, and J. B. Stark, "Nonlinear limits to the information capacity of optical fibre communications," Nature 411, 1027–1030 (2001).

[3] P. J. Winzer, "Making spatial multiplexing a reality," Nat. Photonics 8, 345–348 (2014).

[4] D. Richardson, J. Fini, and L. Nelson, "Space-division multiplexing in optical fibres," Nat. Photonics 7, 354–362 (2013).

[5] R.-J. Essiambre, G. Kramer, P. J. Winzer, G. J. Foschini, and B. Goebel, "Capacity limits of optical fiber networks," J. Lightwave Technol. 28, 662–701 (2010).

[6] C. Kachris, and I. Tomkos, "A survey on optical interconnects for data centers," IEEE Commun. Surv. Tut. 14, 1021–1036 (2012).

[7] K. N. Georgakilas, A. Tzanakaki, M. Anastasopoulos, and J. M. Pedersen, "Converged optical network and data center virtual infrastructure planning," J. Opt. Commun. Netw. 4, 681–691 (2012).

[8] A. Wonfor, H. Wang, R. Penty, and I. White, "Large port count high-speed optical switch fabric for use within datacenters [Invited]," J. Opt. Commun. Netw. 3, A32–A39 (2011).

[9] D. Cotter, R. Manning, K. Blow, A. Ellis, A. Kelly, D. Nesset, I. Phillips, A. Poustie, and D. Rogers, "Nonlinear optics for high-speed digital information processing," Science 286, 1523–1528 (1999).

[10] A. E. Willner, S. Khaleghi, M. R. Chitgarha, and O. F. Yilmaz, "All-optical signal processing," J. Lightwave Technol. 32, 660–680 (2014).

[11] M. Saruwatari, "All-optical signal processing for terabit/second optical transmission," IEEE J. Sel. Top. Quantum Electron. 6, 1363–1374 (2000).

[12] B. J. Eggleton, T. D. Vo, R. Pant, J. Schr, M. D. Pelusi, D. Yong Choi, S. J. Madden, and B. Luther-Davies, "Photonic chip based ultrafast optical processing based on high nonlinearity dispersion engineered chalcogenide waveguides," Laser Photon. Rev. 6, 97–114 (2012).

[13] L. K. Oxenløwe, H. Ji, M. Galili, M. Pu, H. Hu, H. C. H. Mulvad, K. Yvind, J. M. Hvam, A. T. Clausen, and P. Jeppesen, "Silicon photonics for signal processing of Tbit/s serial data signals," IEEE J. Sel. Top. Quantum Electron. 18, 996–1005 (2012).

[14] A. E. Willner, O. F. Yilmaz, J. Wang, X. Wu, A. Bogoni, L. Zhang, and S. R. Nuccio, "Optically efficient nonlinear signal processing," IEEE J. Sel. Top. Quantum Electron. 17, 320–332 (2011).

[15] J. Leuthold, C. Koos, and W. Freude, "Nonlinear silicon photonics," Nat. Photon. 4 (2010).

[16] K. Nozaki, T. Tanabe, A. Shinya, S. Matsuo, T. Sato, H. Taniyama, and M. Notomi, "Sub-femtojoule all-optical switching using a photonic-crystal nanocavity," Nat. Photon. 4, 477–483 (2010).

[17] C. Koos, P. Vorreau, T. Vallaitis, P. Dumon, W. Bogaerts, R. Baets, B. Esembeson, I. Biaggio, T. Michinobu, and F. Diederich, "All-optical high-speed signal processing with silicon–organic hybrid slot waveguides," Nat. Photon. 3, 216–219 (2009).

[18] R. Salem, M. A. Foster, A. C. Turner, D. F. Geraghty, M. Lipson, and A. L. Gaeta, "Signal regeneration using low-power four-wave mixing on silicon chip," Nat. Photon. 2, 35–38 (2008).

[19] C. Langrock, S. Kumar, J. E. McGeehan, A. Willner, and M. Fejer, "All-optical signal processing using χ^2 nonlinearities in guided-wave devices," J. Lightwave Technol. 24, 2579–2592 (2006).

[20] M. Pelusi, F. Luan, E. Magi, M. Lamont, D. Moss, B. Eggleton, J. Sanghera, L. Shaw, and I. Aggarwal, "High bit rate all-optical signal processing in a fiber photonic wire," Opt. Express 16, 11506–11512 (2008).

[21] M. D. Pelusi, V. G. Ta'eed, L. Fu, E. Magi, M. R. Lamont, S. Madden, D.-Y. Choi, D. A. Bulla, B. Luther-Davies, and B. J. Eggleton, "Applications of highly-nonlinear chalcogenide glass devices tailored for high-speed all-optical signal processing," IEEE J. Sel. Top. Quantum Electron. 14, 529–539 (2008).

[22] J. Wang, S. Nuccio, X. Wu, O. F. Yilmaz, L. Zhang, I. Fazal, J.-Y. Yang, Y. Yue, and A. E. Willner, "40 Gbit/s optical data exchange between wavelength-division-multiplexed channels using a periodically poled lithium niobate waveguide," Opt. Lett. 35, 1067–1069 (2010).

[23] J. Wang, and Q. Sun, "Theoretical analysis of power swapping in quadratic nonlinear medium," Appl. Phys. Lett. 96, 081108 (2010).

[24] R. W. Fung, H. K. Cheung, and K. K. Wong, "Widely tunable wavelength exchange in anomalous-dispersion regime," IEEE Photon. Technol. Lett. 19, 1846–1848 (2007).

[25] K. Uesaka, K.-Y. Wong, M. E. Marhic, and L. G. Kazovsky, "Wavelength exchange in a highly nonlinear dispersion-shifted fiber: theory and experiments," IEEE J. Sel. Top. Quantum Electron. 8, 560–568 (2002).

[26] O. F. Yilmaz, J. Wang, S. Khaleghi, X. Wang, S. R. Nuccio, X. Wu, and A. E. Willner, "Preconversion phase modulation of input differential phase-shift-keying signals for wavelength conversion and multicasting applications using phase-modulated pumps," Opt. Lett. 36, 731–733 (2011).

[27] A. Biberman, B. G. Lee, A. C. Turner-Foster, M. A. Foster, M. Lipson, A. L. Gaeta, and K. Bergman, "Wavelength multicasting in silicon photonic nanowires," Opt. Express 18, 18047–18055 (2010).

[28] X. Wu, A. Bogoni, O. F. Yilmaz, S. Nuccio, J. Wang, and A. E. Willner, "Eightfold 40–320 Gbit/s phase-coherent multiplexing and 320–40 Gbit/s demultiplexing using highly nonlinear fibers," Opt. Lett. 35, 1896–1898 (2010).

[29] C.-S. Brès, N. Alic, E. Myslivets, and S. Radic, "Scalable multicasting in one-pump parametric amplifier," J. Lightwave Technol. 27, 356–363 (2009).

[30] H. Hu, H. Ji, M. Galili, M. Pu, C. Peucheret, H. C. H. Mulvad, K. Yvind, J. M. Hvam, P. Jeppesen, and L. K. Oxenløwe, "Ultra-high-speed wavelength conversion in a silicon photonic chip," Opt. Express. 19, 19886–19894 (2011).

[31] S. B. Yoo, "Wavelength conversion technologies for WDM network applications," J. Lightwave Technol. 14, 955–966 (1996).

[32] A. Bogoni, X. Wu, Z. Bakhtiari, S. Nuccio, and A. E. Willner, "640 Gbits/s photonic logic gates," Opt. Lett. 35, 3955–3957 (2010).

[33] A. Bogoni, X. Wu, I. Fazal, and A. E. Willner, "Photonic processing of 320 Gbits/s based on sum-/difference-frequency generation and pump depletion in a single PPLN waveguide," Opt. Lett. 34, 1825–1827 (2009).

[34] A. Bogoni, X. Wu, I. Fazal, and A. E. Willner, "160 Gb/s time-domain channel extraction/insertion and all-optical logic operations exploiting a single PPLN waveguide," J. Lightwave Technol. 27, 4221–4227 (2009).

[35] J. Wang, J. Sun, X. Zhang, D. Huang, and M. Fejer, "Ultrafast all-optical three-input Boolean XOR operation for differential phase-shift keying signals using periodically poled lithium niobate," Opt. Lett. 33, 1419–1421 (2008).

[36] J. Wang, J. Sun, and Q. Sun, "Single-PPLN-based simultaneous half-adder, half-subtracter, and OR logic gate: proposal and simulation," Opt. Express. 15, 1690–1699 (2007).

[37] J. Wang, H. Fu, D. Geng, and A. E. Willner, "Single-PPLN-assisted wavelength-/time-selective switching/dropping/swapping for 100-GHz-spaced WDM signals," Opt. Express. 21, 3756–3774 (2013).

[38] A. Bogoni, X. Wu, S. R. Nuccio, J. Wang, Z. Bakhtiari, and A. E. Willner, "Photonic 640-Gb/s reconfigurable OTDM add–drop multiplexer based on pump depletion in a single PPLN waveguide," IEEE J. Sel. Top. Quantum Electron. 18, 709–716 (2012).

[39] H. Ji, M. Pu, H. Hu, M. Galili, L. K. Oxenløwe, K. Yvind, J. M. Hvam, and P. Jeppesen, "Optical waveform sampling and error-free demultiplexing of 1.28 Tb/s serial data in a nanoengineered silicon waveguide," J. Lightwave Technol. 29, 426–431 (2011).

[40] C. Schubert, C. Schmidt, S. Ferber, R. Ludwig, and H. G. Weber, "Error-free all-optical add-drop multiplexing at 160 Gbit/s," Electron. Lett. 39, 1 (2003).

[41] J. Wang, Z. Bakhtiari, S. R. Nuccio, O. F. Yilmaz, X. Wu, and A. E. Willner, "Phase-transparent optical data exchange of 40 Gbit/s differential phase-shift keying signals," Opt. Lett. 35, 2979–2981 (2010).

[42] N. Alic, E. Myslivets, S. Moro, B.-P. Kuo, R. M. Jopson, C. J. McKinstrie, and S. Radic, "Microsecond parametric optical delays," J. Lightwave Technol. 28, 448–455 (2010).

[43] Y. Dai, Y. Okawachi, A. C. Turner-Foster, M. Lipson, A. L. Gaeta, and C. Xu, "Ultralong continuously tunable parametric delays via a cascading discrete stage," Opt. Express. 18, 333–339 (2010).

[44] S. Nuccio, O. Yilmaz, X. Wang, H. Huang, J. Wang, X. Wu, and A. Willner, "Higher-order dispersion compensation to enable a 3.6 μs wavelength-maintaining delay of a 100 Gb/s DQPSK signal," Opt. Lett. 35, 2985–2987 (2010).

[45] S. Nuccio, O. Yilmaz, X. Wu, and A. Willner, "Fine tuning of conversion/dispersion based optical delays with a 1 pm tunable laser using cascaded acousto-optic mixing," Opt. Lett. 35, 523–525 (2010).

[46] O. F. Yilmaz, S. R. Nuccio, X. Wu, and A. E. Willner, "40-Gb/s optical packet buffer using conversion/dispersion-based delays," J. Lightwave Technol. 28, 616–623 (2010).

[47] Z. Tong, C. Lundström, P. Andrekson, C. McKinstrie, M. Karlsson, D. Blessing, E. Tipsuwannakul, B. Puttnam, H. Toda, and L. Grüner-Nielsen, "Towards ultrasensitive optical links enabled by low-noise phase-sensitive amplifiers," Nat. Photon. 5, 430–436 (2011).

[48] R. Slavík, F. Parmigiani, J. Kakande, C. Lundström, M. Sjödin, P. A. Andrekson, R. Weerasuriya, S. Sygletos, A. D. Ellis, and L. Grüner-Nielsen, "All-optical phase and amplitude regenerator for next-generation telecommunications systems," Nat. Photon. 4, 690–695 (2010).

[49] K. Croussore, and G. Li, "Phase and amplitude regeneration of differential phase-shift keyed signals using phase-sensitive amplification," IEEE J. Sel. Top. Quantum Electron. 14, 648–658 (2008).

[50] M. S. Rasras, I. Kang, M. Dinu, J. Jaques, N. Dutta, A. Piccirilli, M. A. Cappuzzo, E. Y. Chen, L. T. Gomez, and A. Wong-Foy, "A programmable 8-bit optical correlator filter for optical bit pattern recognition," IEEE Photon. Technol. Lett. 20, 694–696 (2008).

[51] J. Wang, Q. Sun, and J. Sun, "All-optical 40 Gbit/s CSRZ-DPSK logic XOR gate and format conversion using four-wave mixing," Opt. Express 17, 12555–12563 (2009).

[52] J. Wang, J. Sun, X. Zhang, D. Huang, and M. Fejer, "Optical phase erasure and its application to format conversion through cascaded second-order processes in periodically poled lithium niobate," Opt. Lett. 33, 1804–1806 (2008).

[53] J. Wang, J. Sun, X. Zhang, D. Huang, and M. M. Fejer, "All-optical format conversions using periodically poled lithium niobate waveguides," IEEE J. Quantum Electron. 45, 195–205 (2009).

[54] J. Wang, J. Sun, Q. Sun, D. Wang, M. Zhou, X. Zhang, D. Huang, and M. M. Fejer, "All-optical format conversion using a periodically poled lithium niobate waveguide and a reflective semiconductor optical amplifier," Appl. Phys. Lett. 91, 051107 (2007).

[55] J. Qiu, K. Sun, M. Rochette, and L. R. Chen, "Reconfigurable all-optical multilogic gate (XOR, AND, and OR) based on cross-phase modulation in a highly nonlinear fiber," IEEE Photon. Technol. Lett. 22, 1199–1201 (2010).

[56] J. Wang, Q. Sun, J. Sun, and X. Zhang, "Experimental demonstration on 40Gbit/s all-optical multicasting logic XOR gate for NRZ-DPSK signals using four-wave mixing in highly nonlinear fiber," Opt. Commun. 282, 2615–2619 (2009).

[57] C. Yu, L. Christen, T. Luo, Y. Wang, Z. Pan, L.-S. Yan, and A. E. Willner, "All-optical XOR gate using polarization rotation in single highly nonlinear fiber," IEEE Photon. Technol. Lett. 17, 1232–1234 (2005).

[58] N. Deng, K. Chan, C.-K. Chan, and L.-K. Chen, "An all-optical XOR logic gate for high-speed RZ-DPSK signals by FWM in semiconductor optical amplifier," IEEE J. Sel. Top. Quantum Electron. 12, 702–707 (2006).

[59] I. Kang, C. Dorrer, and J. Leuthold, "All-optical XOR operation of 40 Gbit/s phase-shift-keyed data using four-wave mixing in semiconductor optical amplifier," Electron. Lett. 40, 496–498 (2004).

[60] J. H. Kim, Y. M. Jhon, Y. T. Byun, S. Lee, D. H. Woo, and S. H. Kim, "All-optical XOR gate using semiconductor optical amplifiers without additional input beam," IEEE Photon. Technol. Lett. 14, 1436–1438 (2002).

[61] J. Wang, Q. Sun, and J. Sun, "Ultrafast all-optical logic AND gate for CSRZ signals using periodically poled lithium niobate," JOSA B 26, 951–958 (2009).

[62] J. Wang, J. Sun, Q. Sun, D. Wang, M. Zhou, X. Zhang, D. Huang, and M. Fejer, "Dual-channel-output all-optical logic AND gate at 20 Gbit/s based on cascaded second-order nonlinearity in PPLN waveguide," Electron. Lett. 43, 1 (2007).

[63] T. D. Vo, R. Pant, M. D. Pelusi, J. Schröder, D.-Y. Choi, S. K. Debbarma, S. J. Madden, B. Luther-Davies, and B. J. Eggleton, "Photonic chip-based all-optical XOR gate for 40 and 160 Gbit/s DPSK signals," Opt. Lett. 36, 710–712 (2011).

[64] J. Hou, L. Chen, W. Dong, and X. Zhang, "40 Gb/s reconfigurable optical logic gates based on FWM in silicon waveguide," Opt. Express 24, 2701-2711 (2016).

[65] N. Ophir, J. Chan, K. Padmaraju, A. Biberman, A. C. Foster, M. Foster, M. Lipson, A. L. Gaeta, and K. Bergman, "Continuous wavelength conversion of 40-Gb/s data over 100 nm using a dispersion-engineered silicon waveguide," IEEE Photon. Technol. Lett. 23, 73–75 (2011).

[66] H. Rong, Y.-H. Kuo, A. Liu, M. Paniccia, and O. Cohen, "High efficiency wavelength conversion of 10 Gb/s data in silicon waveguides," Opt. Express 14, 1182–1188 (2006).

[67] X. Hu, M. Zeng, A. Wang, L. Zhu, L. Fu, and J. Wang, "Graphene-assisted nonlinear optical device for four-wave mixing based tunable wavelength conversion of QPSK signal," Opt. Express 23, 26158–26167 (2015).

[68] P. J. Winzer, G. Raybon, H. Song, A. Adamiecki, S. Corteselli, A. H. Gnauck, D. A. Fishman, C. R. Doerr, S. Chandrasekhar, and L. L. Buhl, "100-Gb/s DQPSK transmission: From laboratory experiments to field trials," J. Lightwave Technol. 26, 3388–3402 (2008).

[69] P. Guan, T. Hirano, K. Harako, Y. Tomiyama, T. Hirooka, and M. Nakazawa, "2.56 Tbit/s/ch polarization-multiplexed DQPSK transmission over 300 km using time-domain optical Fourier transformation," Opt. Express 19, B567–B573 (2011).

[70] J. Wang, S. R. Nuccio, J.-Y. Yang, X. Wu, A. Bogoni, and A. E. Willner, "High-speed addition/subtraction/complement/doubling of quaternary numbers using optical nonlinearities and DQPSK signals," Opt. Lett. 37, 1139–1141 (2012).

[71] J. Wang, J.-Y. Yang, H. Huang, and A. E. Willner, "Three-input optical addition and subtraction of quaternary base numbers," Opt. Express 21, 488–499 (2013).

[72] A. Wang, X. Hu, L. Zhu, M. Zeng, L. Fu, and J. Wang, "Experimental demonstration on two-input optical high-base hybrid doubling and subtraction functions in graphene," Opt. Express 23, 31728–31735 (2015).

[73] C. Gui, and J. Wang, "Silicon Waveguide based Two-Input Simultaneous Quaternary Hybrid Doubling/Subtraction (2A-B, 2B-A) Using Degenerate FWM and QPSK," in *CLEO*: *Applications and Technology* (Optical Society of America, 2015), paper JTu5A. 45.

[74] Y. Long, C. Gui, A. Wang, X. Hu, L. Zhu, L. Zhou, and J. Wang, "All-Optical Three-Input Simultaneous Multicasted Quaternary Addition/Subtraction Using Non-degenerate FWM in a Silicon Waveguide and 20 Gibt/s QPSK Signal," in *Optical Fiber Communication Conference* (Optical Society of America, 2016), paper Th2A. 6.

[75] A. Wang, Y. Long, L. Zhu, L. Zhou, and J. Wang, "Silicon Waveguide based Two-Input Octal Addition/Subtraction Using Non-Degenerate FWM and 8PSK," in *Asia Communications and Photonics Conference* (Optical Society of America, 2015), paper AM4A. 5.

[76] L. Lei, J. Dong, B. Zou, Z. Wu, W. Dong, and X. Zhang, "Expanded all-optical programmable logic array based on multi-input/output canonical logic units," Opt. Express 22, 9959–9970 (2014).

[77] L. Lei, J. Dong, Y. Yu, S. Tan, and X. Zhang, "All-optical canonical logic units-based programmable logic array (CLUs-PLA) using semiconductor optical amplifiers," J. Lightwave Technol. 30, 3532–3539 (2012).

[78] H. Chen, G. Zhu, Q. Wang, J. Jaques, J. Leuthold, A. Piccirilli, and N. Dutta, "All-optical logic XOR using differential scheme and Mach-Zehnder interferometer," Electron. Lett. 38, 1 (2002).

[79] J.-Y. Kim, J.-M. Kang, T.-Y. Kim, and S.-K. Han, "All-optical multiple logic gates with XOR, NOR, OR, and NAND functions using parallel SOA-MZI structures: theory and experiment," J. Lightwave Technol. 24, 3392 (2006).

[80] A. Bogoni, L. Poti, R. Proietti, G. Meloni, F. Ponzini, and P. Ghelfi, "Regenerative and reconfigurable all-optical logic gates for ultra-fast applications," Electron. Lett. 41, 1 (2005).

[81] T. A. Ibrahim, R. Grover, L. Kuo, S. Kanakaraju, L. Calhoun, and P. Ho, "All-optical AND/NAND logic gates using semiconductor microresonators," IEEE Photon. Technol. Lett. 15, 1422–1424 (2003).

[82] Z. Li, and G. Li, "Ultrahigh-speed reconfigurable logic gates based on four-wave mixing in a semiconductor optical amplifier," IEEE Photon. Technol. Lett. 18, 1341 (2006).

[83] Q. Xu, and M. Lipson, "All-optical logic based on silicon micro-ring resonators," Opt. Express 15, 924–929 (2007).

[84] T. Fjelde, D. Wolfson, A. Kloch, B. Dagens, A. Coquelin, I. Guillemot, F. Gaborit, F. Poingt, and M. Renaud, "Demonstration of 20 Gbit/s all-optical logic XOR in integrated SOA-based interferometric wavelength converter," Electron. Lett. 36, 1863–1864 (2000).

[85] F. Li, T. Vo, C. Husko, M. Pelusi, D.-X. Xu, A. Densmore, R. Ma, S. Janz, B. Eggleton, and D. Moss, "All-optical XOR logic gate for 40Gb/s DPSK signals via FWM in a silicon nanowire," Opt. Express 19, 20364–20371 (2011).

[86] L. Lei, J. Dong, Y. Zhang, H. He, Y. Yu, and X. Zhang, "Reconfigurable photonic full-adder and full-subtractor based on three-input XOR gate and logic minterms," Electron. Lett. 48, 399–400 (2012).

[87] B. Dai, S. Shimizu, X. Wang, and N. Wada, "Simultaneous all-optical half-adder and half-subtracter based on two semiconductor optical amplifiers," IEEE Photon. Technol. Lett. 25, 91–93 (2013).

[88] J. E. McGeehan, S. Kumar, and A. E. Willner, "Simultaneous optical digital half-subtraction and-addition using SOAs and a PPLN waveguide," Opt. Express 15, 5543–5549 (2007).

[89] S. H. Kim, J. H. Kim, J. W. Choi, C. W. Son, Y. T. Byun, Y. M. Jhon, S. Lee, D. H. Woo, and S. H. Kim, "All-optical half adder using cross gain modulation in semiconductor optical amplifiers," Opt. Express 14, 10693–10698 (2006).

[90] S. Kumar, A. E. Willner, D. Gurkan, K. R. Parameswaran, and M. M. Fejer, "All-optical half adder using an SOA and a PPLN waveguide for signal processing in optical networks," Opt. Express 14, 10255–10260 (2006).

[91] J. H. Kim, Y. T. Byun, Y. M. Jhon, S. Lee, D. H. Woo, and S. H. Kim, "All-optical half adder using semiconductor optical amplifier based devices," Opt. Commun. 218, 345–349 (2003).

[92] S. Iijima, and T. Ichihashi, "Single-shell carbon nanotubes of 1-nm diameter," Nature, 363, 603-605 (1993).

[93] A. K. Geim, and K. S. Novoselov, "The rise of graphene," Nat. Mater. 6, 183–191 (2007).

[94] D. Basko, "A photothermoelectric effect in graphene," Science 334, 610–611 (2011).

[95] L. Wang, W. Cai, X. Zhang, and J. Xu, "Surface plasmons at the interface between graphene and Kerr-type nonlinear media," Opt. Lett. 37, 2730–2732 (2012).

[96] Z. Sun, T. Hasan, F. Torrisi, D. Popa, G. Privitera, F. Wang, F. Bonaccorso, D. M. Basko, and A. C. Ferrari, "Graphene mode-locked ultrafast laser," ACS Nano 4, 803–810 (2010).

[97] H. Zhou, T. Gu, J. F. McMillan, N. Petrone, A. van der Zande, J. C. Hone, M. Yu, G. Lo, D.-L. Kwong, and G. Feng, "Four-wave mixing in slow-light graphene-silicon photonic crystal waveguides," in *2014 Conference on Lasers and Electro-Optics* (*CLEO*)-*Laser Science to Photonic Applications*(IEEE, 2014), paper 1–2.

[98] B. Xu, A. Martinez, K. Fuse, and S. Yamashita, "Generation of four wave mixing in graphene and carbon nanotubes optically deposited onto fiber ferrules," in *CLEO*: *Science and Innovations* (Optical Society of America, 2011), paper CMAA6.

[99] Y. Wu, B. Yao, Y. Cheng, Y. Rao, Y. Gong, X. Zhou, B. Wu, and K. S. Chiang, "Four-wave mixing in a microfiber attached onto a graphene film," IEEE Photon. Technol. Lett. 26, 249–252 (2014).

[100] B. Xu, A. Martinez, and S. Yamashita, "Mechanically exfoliated graphene for four-wave-mixing-based wavelength conversion," IEEE Photon. Technol. Lett. 20, 1792–1794 (2012).

[101] C. Gui, and J. Wang, "Silicon-organic hybrid slot waveguide based three-input multi-casted optical hexadecimal addition/subtraction," Sci. Rep. 4 (2014).

IntechOpen